CANCER

Cervical extracellular matrix hydrogel optimizes tumor heterogeneity of cervical squamous cell carcinoma organoids

Haonan Song[1]†, Haoyuan Jiang[1]†, Weichu Hu[1]†, Yan Hai[1], Yihuan Cai[1], Hu Li[2], Yuru Liao[1], Yi Huang[3], Xiaogang Lv[4], Yefei Zhang[1], Jiping Zhang[5], Yan Huang[6], Xiaomei Liang[1], Hao Huang[3]*, Xinhua Lin[7,8]*, Yifeng Wang[1]*, Xiao Yi[1,7]*

Cervical cancer, primarily squamous cell carcinoma, is the most prevalent gynecologic malignancy. Organoids can mimic tumor development in vitro, but current Matrigel inaccurately replicates the tissue-specific microenvironment. This limitation compromises the accurate representation of tumor heterogeneity. We collected paracancerous cervical tissues from patients diagnosed with cervical squamous cell carcinoma (CSCC) and prepared uterine cervix extracellular matrix (UCEM) hydrogels. Proteomic analysis of UCEM identified several tissue-specific signaling pathways including human papillomavirus, phosphatidylinositol 3-kinase–AKT, and extracellular matrix receptor. Secreted proteins like FLNA, MYH9, HSPA8, and EEF1A1 were present, indicating UCEM successfully maintained cervical proteins. UCEM provided a tailored microenvironment for CSCC organoids, enabling formation and growth while preserving tumorigenic potential. RNA sequencing showed UCEM-organoids exhibited greater similarity to native CSCC and reflected tumor heterogeneity by exhibiting CSCC-associated signaling pathways including virus protein-cytokine, nuclear factor κB, tumor necrosis factor, and oncogenes EGR1, FPR1, and IFI6. Moreover, UCEM-organoids developed chemotherapy resistance. Our research provides insights into advanced organoid technology through native matrix hydrogels.

INTRODUCTION

Cervical cancer is the most common gynecological malignancy and a leading cause of cancer-related death in women, particularly in countries with low development indices (*1*, *2*). Although human papillomavirus (HPV) has been identified as the primary cause of cervical cancer, and worldwide efforts are being made to eradicate the disease through HPV vaccination and early screening, a notable number of patients are still being diagnosed each year. Cervical squamous cell carcinoma (CSCC) is the predominant tissue type of cervical cancer, accounting for more than 70% (*3*). Surgery, radiotherapy, and comprehensive chemotherapy offer limited success in curing patients and often come with significant side effects and risk of complications, making precise medical treatment elusive. Cancer cell lines and tumor tissue xenotransplantation models commonly used in research fail to accurately replicate the native pathological state of human CSCC in vitro due to the absence of the specific microenvironment of human cervical tissue. Therefore, reproducing tumor occurrence in vitro remains challenging (*4*, *5*). Consequently, these limitations hinder drug development trials and the realization of precision medicine.

Organoids are three-dimensional microorganisms that closely resemble the structure of their source organs and can partially replicate the physiological and pathological characteristics of native tissues, making them a powerful pathological model for tumor-related studies (*6*, *7*). Currently, the culture of organoids heavily relies on Matrigel, a substance derived from the extract of basal membrane proteins present in EHS mouse osteosarcoma. Laminin is the major component of Matrigel (*8*). Nevertheless, Matrigel has a number of limitations in accurately reflecting human pathology: (i) Due to the distinct microenvironments required for the growth of different tumor cells, Matrigel fails to effectively provide tissue-specific microenvironments for organoids from different tissues, and there are also species differences (*8*, *9*). (ii) In terms of biochemical composition, Matrigel lacks the high proportion of collagen fibers found in CSCC tumor tissues (*10*). These factors collectively result in a deficiency in representing tumor heterogeneity and an inadequate reflection of individual differences. Notably, changes in extracellular matrix (ECM) properties have a profound effect on cell phenotype in vivo. Organoids constructed using ECM derived from native tissue exhibit a greater similarity to the real pathological and physiological state in vivo (*11*, *12*). For instance, Saheli *et al.* (*13*) used liver-derived ECM to culture liver organoids, displaying higher cell viability and significant upregulation of hepatocyte-specific transcriptional products and functions. The ECM not only provides structural support but also contains multiple cytokines and proteins from extracellular vesicles (EVs), which are critical for reconstructing the physiological structure and function of the source tissue. Collagen proteins, proteoglycans, and glycoproteins present in brain ECM (BEM) can influence neuronal polarization, migration, axon growth, and synaptic development. However, Matrigel lacks these directional induction effects

[1]Department of Gynecology, Zhujiang Hospital, Southern Medical University, Guangzhou 510280, China. [2]The First Affiliated Hospital, Jinan University, Guangzhou 510280, China. [3]Department of Gynecology, The Sixth Affiliated Hospital, South China University of Technology, Foshan 528200, China. [4]Department of Gynecologic Oncology, Affiliated Cancer Hospital and Institute of Guangzhou Medical University, Guangzhou 510030, China. [5]Department of Gynecology, Affiliated Foshan Maternity & Child Healthcare Hospital, Southern Medical University, Foshan, China. [6]Second Department of Hepatobiliary Surgery, Zhujiang Hospital, Southern Medical University, Guangzhou 510280, China. [7]Greater Bay Area Institute of Precision Medicine, Guangzhou 510280, China. [8]State Key Laboratory of Genetic Engineering, School of Life Sciences, Zhongshan Hospital, Fudan University Shanghai, Shanghai 200438, China.
*Corresponding author. Email: fshaos@163.com (H.H.); xlin@fudan.edu.cn (X.L.); wangyifeng@smu.edu.cn (Y.W.); yixiao9309@163.com (X.Y.)
†These authors contributed equally to this work.

(*14*). In contrast, small intestinal organoids cultured in intestinal-derived ECM hydrogels are not only capable of forming small intestinal structures, such as crypts and villi, but also have a significantly higher proportion of crypt stem cells compared to those cultured in Matrigel (*15*). Kim *et al.* (*16*) also demonstrated that the ECM derived from the small intestine is better suited for the growth of small intestinal organoids. Furthermore, gastrointestinal organoids cultured in decellularized hydrogels of gastrointestinal tissues exhibit high viability, whereas significant cell death is observed in decellularized hydrogels derived from other tissues like skin, lymph, heart, and muscle. This result highlights the tissue-specific effects of the ECM microenvironment on organoid development (*17*). There exists a process of mutual adaptation between tumor cells and the surrounding environment, which hinges on the direct contact between tumor cells and matrix components, as well as biochemical signaling factors in the microenvironment. The ECM in various tissues has tissue-specific structural components and signaling factors that regulate cell adhesion, migration, proliferation, and differentiation, leading to the guidance of cellular activity processes and development. Thus, in research, it is imperative to evaluate tumors as complete organs rather than merely studying them as individual tumor cells (*18*, *19*). Research models that disregard the tissue-specific biological microenvironment of tumors fail to accurately reflect tumor heterogeneity. All of these factors highlight the significance of tissue-specific ECM microenvironments for organoid culture and also suggest that Matrigel cannot serve as a universal substitute for the ECM. The use of ECM materials derived from native tissues to construct native tumor organoids proves to be more conducive to replicating the biological behavior of tumor cells and more closely resembling the real pathological and physiological states in vivo.

In this study, we collected para-cancer cervical tissue from patients diagnosed with CSCC and used it to prepare uterine cervix ECM (UCEM) hydrogels. UCEM exhibited specific proteomic characteristics of cervical tissue, preserving the structural components of cervical ECM, as well as signaling pathways and secreted proteins associated with carcinogenesis. Our experimental findings demonstrated that UCEM-induced transcriptional characteristics of CSCC organoids closely resembled those of the patients' native CSCC tissues, retaining a higher presence of oncogenes and signaling pathways linked to CSCC. This similarity with native CSCC proved advantageous in capturing the tumor heterogeneity of CSCC (Fig. 1).

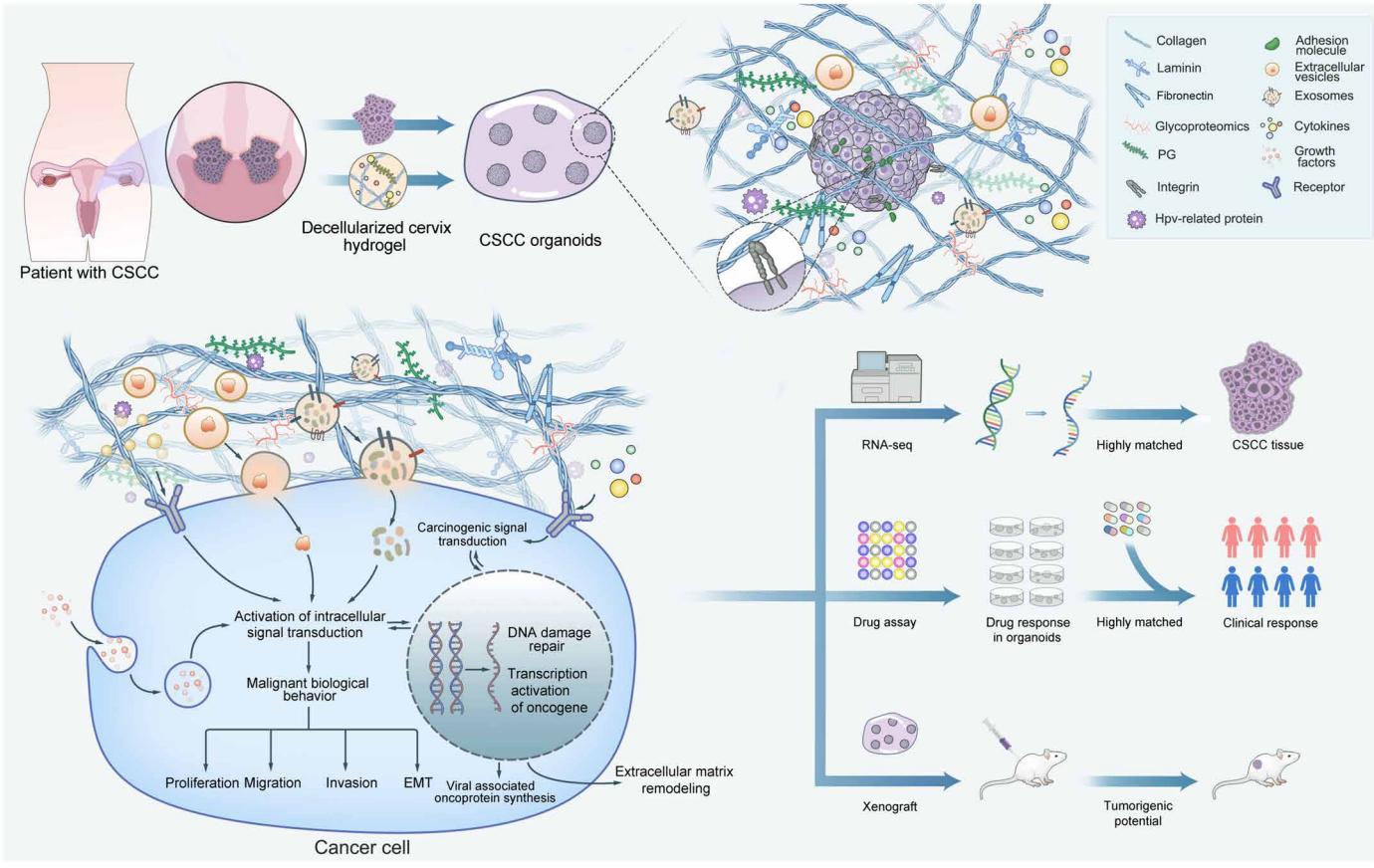

Fig. 1. The construction of CSCC organoids using UCEM hydrogels enables the representation of tumor heterogeneity. UCEM is prepared through the decellularization technique, containing both the structural components (collagen, fibronectin, and laminin) and functional components (cytokines and secreted proteins involved in cellular activities) of the cervical extracellular matrix. This composition preserves the specific microenvironment of cervical tissue. On the basis of this foundation, CSCC organoids were constructed using UCEM. Consequently, UCEM influences the metabolism of tumor cells within CSCC organoids, leading to the promotion of CSCC oncogene expression. Moreover, UCEM is partially associated with the resistance of organoids to chemotherapy drugs. The in vitro drug response of UCEM-organoids is correlated with the clinical response observed in patients. In summary, organoids cultured within UCEM closely resemble the pathophysiological status of cervical cancer tissue in vivo, thus effectively reflecting the tumor heterogeneity in CSCC. EMT, epithelial-mesenchymal transition; RNA-seq, RNA sequencing.

RESULTS

Decellularization and gelation of para-cancer cervical tissue

A hydrogel of human uterine cervical ECM was prepared using decellularization techniques. Following our previous reports, the cervical tissue was minced and decellularized, followed by sterilization, lyophilization, and grinding into a powder. Digestion with hydrochloric acid pepsin yielded a pre-gel. UCEM was obtained through neutralization with sodium hydroxide (Fig. 2A). The synthesized UCEM exhibited high transparency and reduced impurities. After incubation at 37°C for 20 to 30 min, they solidified into hemispherical droplet-shaped structures, providing a reliable three-dimensional environment for cell growth. Analysis through hematoxylin and eosin (H&E) staining, Masson staining, and immunofluorescence demonstrated the removal of most cellular components (CCs) after decellularization while preserving crucial ECM components, such as type I and IV collagen fibers, laminin β1, and fibronectin (Fig. 2B). Quantification of DNA content revealed a substantial decrease from 4048.34 ± 270.72 ng/mg in the cervical tissue before decellularization to 20.78 ± 4.98 ng/mg in decellularized tissue, indicating a significant reduction in DNA after the decellularization process (Fig. 2C). Moreover, the dry weight of the decellularized cervix decreased significantly in comparison to the fresh native tissue (Fig. 2D). Decellularization led to the removal of intact cells and nuclei, eliminating most of the CCs. Further investigation into the microstructure of UCEM demonstrated the formation of a dense network through cross-linking of collagen fibers (Fig. 2E). At 37°C, UCEM exhibited a higher storage modulus (G′) than loss modulus(G″), indicating the successful formation of a stable ECM network with high viscoelasticity and mechanical strength (fig. S1). These findings indicate the successful removal of cell components while retaining key ECM structural components, resulting in a relatively intact ECM morphology.

UCEM preservation of the distinctive cervical ECM Microenvironment

Mass spectrometry is the primary method for studying proteomics. To gain further insights into the proteomics of UCEM, we used mass

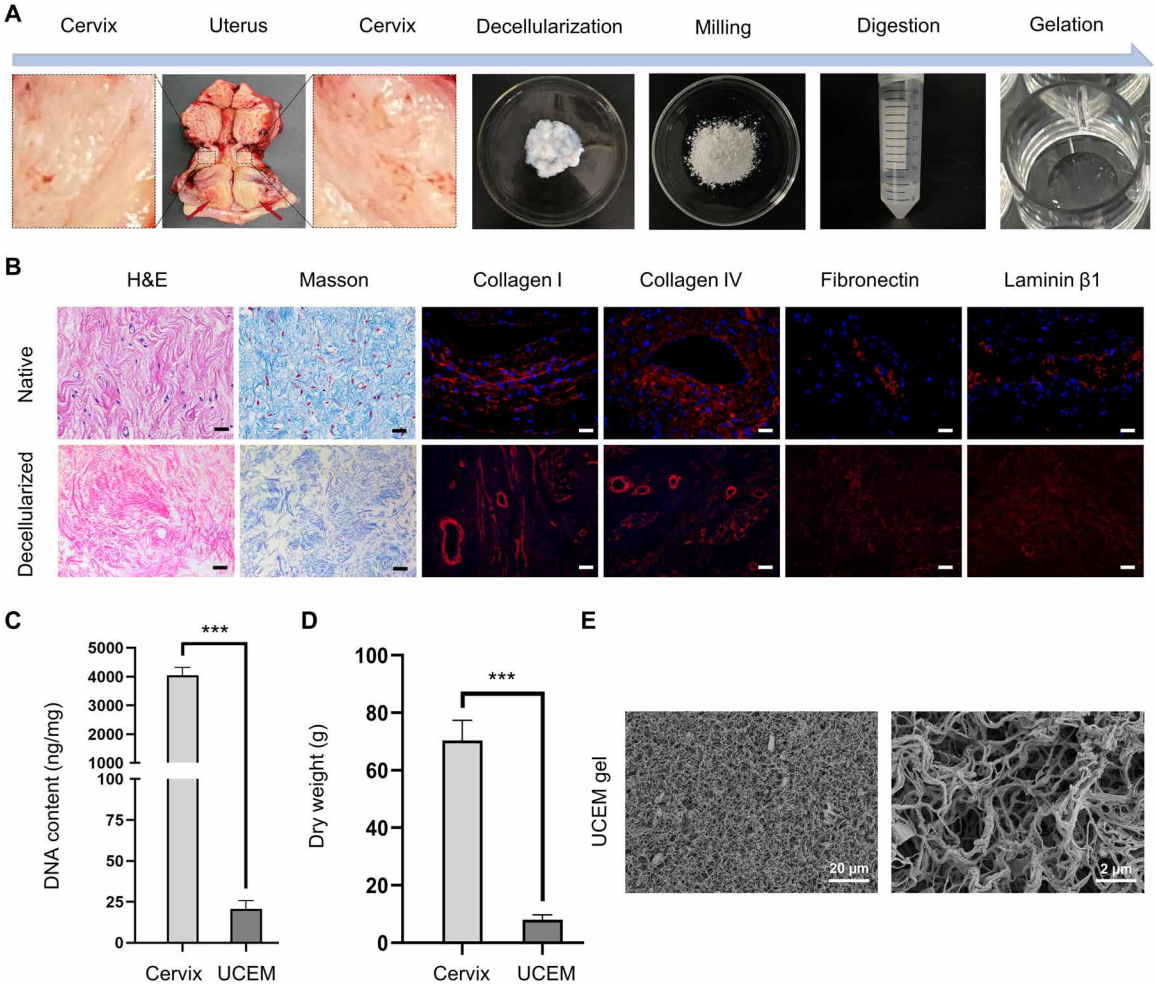

Fig. 2. Preparation of the human cervix–derived extracellular matrix hydrogel (UCEM) by decellularization. (**A**) Preparation process of human cervical derived ECM hydrogel (the arrow showed a squamous cell carcinoma of the cervix). (**B**) Comparison of cervical tissue before and after decellularization. Hematoxylin and eosin (H&E) staining showed that the acidophilic collagen fibers of the cervix after decellularization were stained pink. Masson staining showed collagen fibers dyed blue. Immunofluorescence staining showed collagen I, collagen IV, fibronectin, and laminin β1 in the cervix before and after decellularization. The blue fluorescence represents DAPI staining of the cell nuclei. Scale bars, 25 μm. (**C**) Changes of DNA content (in nanograms per milligram) in cervical tissues before and after decellularization. (**D**) Changes in dry weight (in grams) of cervical tissue before and after decellularization. (**E**) Scanning electron microscopy showed that collagen fibers were interconnected into a network in UCEM. ***$P < 0.001$.

spectrometry to identify and analyze the protein constituents of UCEM (data S1). In three biological replicates, a total of 1368 proteins were identified, surpassing the number found in Matrigel (Fig. 3A and fig. S2A). In addition, UCEM exhibited a higher abundance of human cervical tissue–specific proteins compared to Matrigel (fig. S2B). The core matrisome analysis revealed the presence of various human ECM core matrisome and core matrisome–related proteins in UCEM, including collagen, glycoproteins, proteoglycans, ECM regulators, ECM-affiliated proteins, and secreted factors (fig. S3A). Functional classification of these proteins, based on the clusters of orthologous groups of proteins (COG)/eukaryotic orthologous groups (KOG) database, predominantly linked them to protein modification, signal transduction, and vesicle transport (fig. S4). Further analysis using Gene Ontology (GO) enrichment indicated that the proteins within UCEM played a dual role, serving as both the structural support of the ECM and participating in intracellular metabolism and cell-ECM interactions (Fig. 3E). In the biological process (BP) group, protein functions were mainly associated with nutrition, energy metabolism, and nucleotide metabolism, including processes such as citrate metabolism, tricarboxylic acid metabolism, ribonucleoside triphosphate metabolism, and purine nucleoside triphosphate metabolism. The CC group predominantly concentrated on intracellular and EVs, as well as the ECM, exemplified by the cytoplasmic vesicle lumen, secretory granule lumen, ECM, and secretory vesicle. The molecular function (MF) group primarily engaged in metabolic complex composition and enzyme activity regulation, involving functions such as purine nucleoside binding, nucleoside phosphate binding, nucleotide binding, carbohydrate derivative binding, and nucleoside triphosphatase activity. Moreover, Kyoto Encyclopedia of Genes and Genomes (KEGG) enrichment analysis demonstrated significant enrichment of UCEM protein components in focal adhesion, ECM-receptor interaction, PI3K-AKT signaling pathway, and HPV (Fig. 3B). These signaling pathways play crucial roles in cell adhesion, proliferation, motility, and morbidity. The focal adhesion pathway facilitates cytoskeletal reorganization, adhesion, and migration, which are vital for cell adhesion and localization (*20*, *21*). The interaction between ECM and receptors plays a crucial role in converting extracellular signals into intracellular BPs and regulating the invasion and metastasis of tumor cells (*22*, *23*). The PI3K-AKT signaling pathway is activated in a wide range of tumors and is involved in cell metabolism, protein synthesis, cytoskeletal reorganization, as well as the regulation of cell proliferation, survival, and differentiation processes (*24*, *25*). HPV is considered the primary cause of cervical cancer. UCEM preserved the HPV infection-related signaling pathway, essential for researching the pathogenesis and treatment of cervical cancer caused by HPV. The protein abundance analysis revealed that UCEM contained high levels of collagen (types I, IV, and VI) and basement membrane components (such as proteoglycans and glycoproteins) that closely resembled those found in human tissues (Fig. 3C). In addition, a significant number of secreted and exosomal proteins exist (Fig. 3D), playing pivotal roles in the proliferation, invasion, and metastasis of CSCC. Note that UCEM preserved essential structural components of the ECM as well as protein components crucial for cellular activities. This preservation is advantageous in unraveling the intricate interplay between tumors and the ECM. The protein components of UCEM were found to be distributed in groups through protein interaction analysis. For analysis, we selected five groups that exhibited a high degree of interaction. The central proteins identified, as shown in fig. S3B, were primarily ECM structural proteins such as VCL, ACTG1, HNRNPK, FN1, and HSP90AA1. Fibronectin 1 (FN1) is a key constituent of the ECM, contributing to cell adhesion and migration. It plays a role in improving the motility of cancer cells and is closely implicated in the invasion and metastasis of CSCC (*26*). The up-regulation of HSP90AA1 in cervical cancer tissues is specifically linked to the development of chemotherapy and radiotherapy resistance (*27*). These findings suggest that UCEM not only contributes to the provision of ECM structural components necessary for cell growth but also retains cell factors and tissue-specific proteins associated with cellular activities such as energy metabolism and signal transduction from native tissues. Consequently, UCEM could preserve a cervix tissue-specific ECM microenvironment that is absent in other ECM sources like Matrigel.

Supporting the formation and growth of CSCC organoids with UCEM

We collected a total of 52 cases of CSCC, and the general information of the patients is presented in table S1. This table contains recorded information regarding the patient's age, HPV infection type, clinical stage (FIGO 2018), and tumor size. After digestion and filtration, CSCC cells were embedded and solidified in Matrigel and UCEM, and then added to the culture medium for CSCC organoids. CSCC organoids were observed in both UCEM and Matrigel after 7 to 10 days. Tumor cells from 31 patients self-organized to form CSCC organoids in Matrigel (59.62%) and were able to form organoids in UCEM from 34 patients (65.38%). Among them, four were only formed in Matrigel, seven were only present in UCEM, and the rest were cultured in both mediums (Fig. 4, A and B). The success rate of organoid culture in the two groups was analyzed using a chi-square test, which showed no statistically significant difference ($\chi^2 = 0.369$, $P > 0.05$). This indicates that UCEM can achieve a similar success rate to Matrigel in the organoid culture of CSCC. We observed a lower efficiency of organoid formation in UCEM compared to Matrigel (Fig. 4C). Then, we compared and analyzed the differences in protein components and content between UCEM and Matrigel (fig. S5). The results showed that the content of laminin in UCEM was significantly lower than that in Matrigel. Laminin may be a crucial factor affecting organoid formation efficiency. Laminin is a major component of the basement membrane, consisting of three distinct chains (α, β, and γ) that provide a structural scaffold for the ECM (*28*). Different combinations of α, β, and γ chains form various laminin isoforms. We further analyzed the proteomics of UCEM to clarify the possible laminin isoforms present in UCEM. The laminin subunits detected in UCEM include LAMA2, LAMA3, LAMA4, LAMA5, LAMB1, LAMB2, and LAMC1. The possible laminin isoforms include (fig. S6, A to D) laminin2/211, laminin4/221, laminin6/311, laminin7/321, laminin8/411, laminin9/421, laminin10/511, and laminin11/521. Dysregulation of cell-laminin interactions is a key feature of many cancers (*29*). Certain members of the laminin family, including laminin-521/332/111, play more complex roles in tumor survival, cancer cell migration, and tumor invasion (*30*–*32*). Laminin-521 is involved not only in maintaining embryonic stem cells and inducing pluripotent stem cells but also in cancer self-renewal and invasion (*32*). Therefore, we supplemented UCEM with varying concentrations of laminin-521 (rhLaminin-521, Gibco, A29248) and assessed the formation efficiency of CSCC organoids. As depicted in Fig. 4C, the efficiency of organoid formation in UCEM increased with an elevation in laminin-521 concentration. However, no further improvement in organoid formation efficiency was observed beyond a laminin-521 concentration of 0.1 mg/ml. Nevertheless, the organoid formation efficiency in UCEM remained

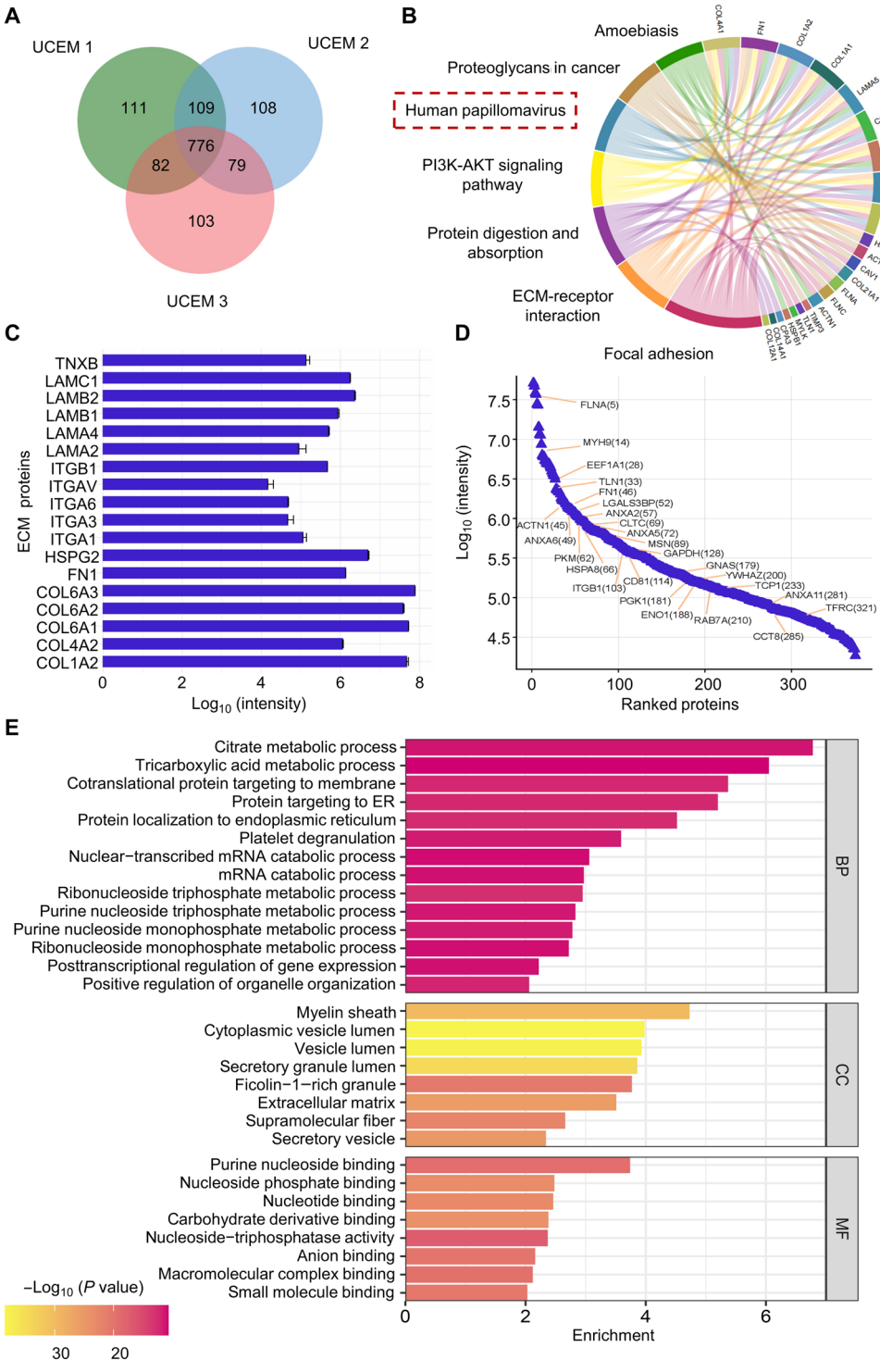

Fig. 3. Mass spectrometry detection and bioinformatics analysis of UCEM. (**A**) The Venn diagram of UCEM proteins identified in three biological replicates. (**B**) Kyoto Encyclopedia of Genes and Genomes (KEGG) pathway enrichment analysis of UCEM showed significant enrichment in HPV pathways related to the development of cervical cancer, in addition to cell adhesion and ECM-receptor interaction. (**C**) Protein abundance analysis revealed structural components of ECM (including collagen, proteoglycan, laminin, and fibronectin) in UCEM. (**D**) Protein abundance analysis revealed secretory and exosome proteins in UCEM. (**E**) UCEM protein component Gene Ontology (GO) enrichment analysis. BP, biological process; CC, cellular component; MF, molecular function.

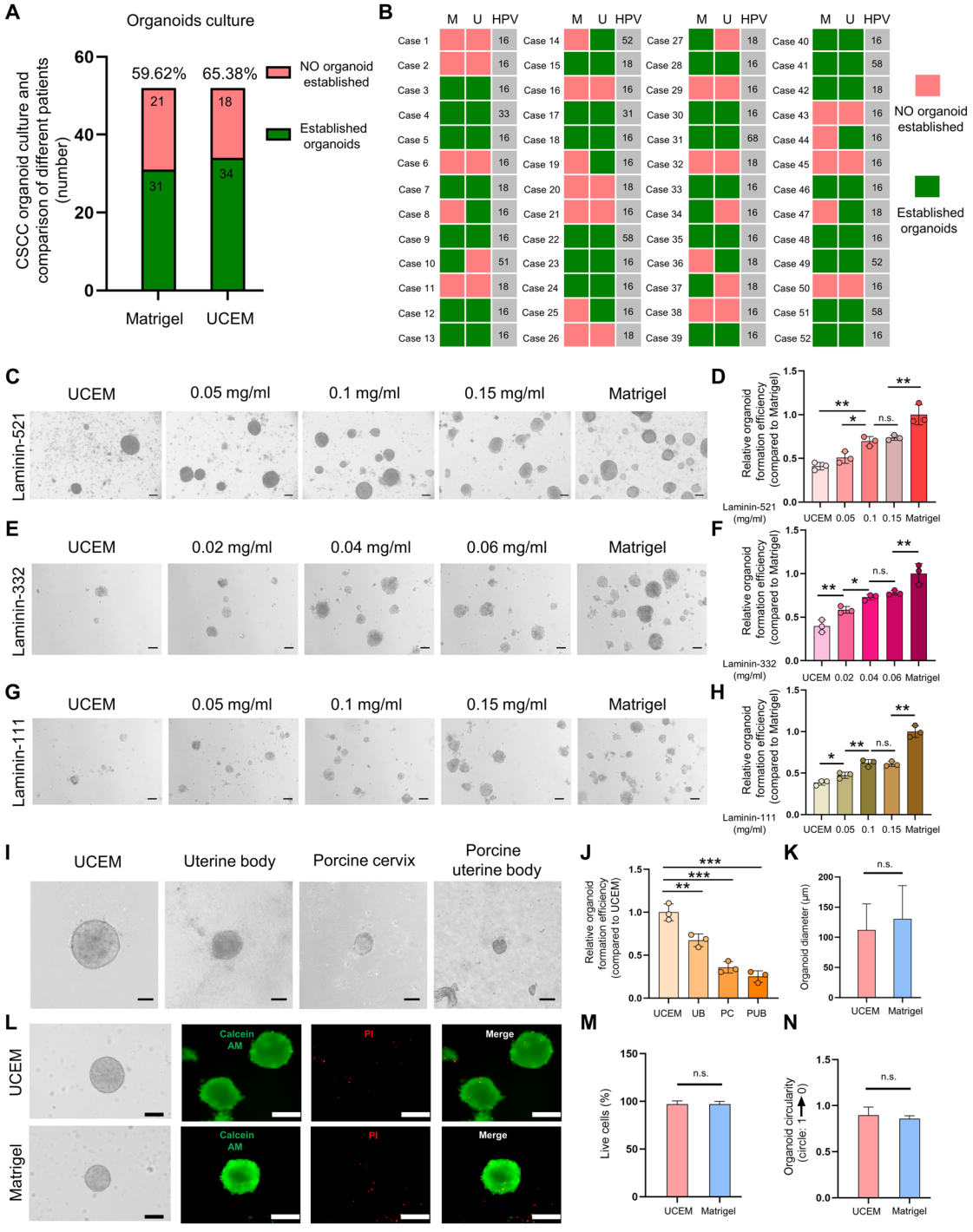

Fig. 4. CSCC organoids cultured in UCEM and Matrigel and comparison. (**A**) Comparison of the success rate of CSCC organoid culture between UCEM and Matrigel. (**B**) Culture of CSCC organoids in UCEM and Matrigel. M represents Matrigel, U represents UCEM, and HPV represents human papillomavirus. (**C**) CSCC organoids cultured in UCEM with the addition of different concentrations of laminin-521. Scale bars, 100 μm. (**D**) Effect of different concentrations of laminin-521 on the efficiency of organoid formation in UCEM. (**E**) CSCC organoids cultured in UCEM supplemented with different concentrations of laminin-332. Scale bars, 100 μm. (**F**) Effect of different concentrations of laminin-332 on organoid formation efficiency in UCEM. (**G**) CSCC organoids cultured in UCEM supplemented with different concentrations of laminin-111. Scale bars, 100 μm. (**H**) Effect of different concentrations of laminin-111 on organoid formation efficiency in UCEM. (**I**) CSCC organoids cultured in ECM hydrogels from different tissues. Scale bars, 100 μm. (**J**) Comparison of organoid formation efficiency in ECM hydrogels from different tissues. UCEM, uterine cervix extracellular matrix; UB, uterine body; PC, porcine cervix; PUB, porcine uterine body. (**K**) Comparison of organoids diameters in UCEM and Matrigel; $P > 0.05$. (**L**) CSCC organoids cultured in UCEM and Matrigel and live/dead cell staining of organoids. Scale bars, 100 μm. PI, propidium iodide. (**M**) Comparison of the percentage of living cells in CSCC organoids cultured in UCEM and Matrigel; $P > 0.05$. (**N**) Comparison of circularity of CSCC organoids in UCEM and Matrigel (the closer the ratio of the short axis to the long axis is to 1, the more circular the morphology). n.s., not significant.*$P < 0.05$; **$P < 0.01$; ***$P < 0.001$.

lower than that in Matrigel, with a statistically significant difference ($P < 0.01$) (Fig. 4D). Laminin-332 can serve as a marker for early invasion of cervical cancer and facilitates HPV infection and replication (*33*, *34*). Laminin-111 is a laminin isoform with a high content in Matrigel (*9*, *35*) and may be an important factor affecting organoid formation. In addition, the expression of laminin-111 is increased by 3.8-fold in CSCC compared with normal cervical tissue (*36*). We conducted additional experiments targeting laminin isoforms to further investigate the effects of laminin-332 and laminin-111 on CSCC organoid formation. The results showed that with the increase in laminin-332 and laminin-111 concentrations, the formation efficiency of CSCC organoids was improved, reaching a peak at 0.04 and 0.1 mg/ml, respectively (Fig. 4, E to H). These results indicate that UCEM can support the formation of CSCC organoids, while laminin can enhance their formation efficiency. The simultaneous addition of multiple laminins could potentially further enhance the formation efficiency of CSCC organoids, possibly reaching the level of Matrigel. Scanning electron microscopy further revealed the presence of collagen and other protein components surrounding the CSCC organoids. Notably, collagen exhibited a mesh-like distribution, while other proteins were dispersed (fig. S7). Furthermore, to examine the influence of tissue-specific microenvironments on organoid formation, we cultured CSCC organoids using ECM hydrogels derived from the human uterine body (UB), porcine cervix (PC), and porcine UB (PUB), and compared them to UCEM. The findings demonstrated that CSCC organoids could maintain a robust morphology in both UCEM and UB, whereas, in PC and PUB, they exhibited smaller sizes and struggled to maintain a stable sphere-like structure (Fig. 4I). Comparative analysis of organoid formation efficiency revealed that UCEM exhibited the highest efficiency in CSCC organoid formation (Fig. 4J). These results highlight the influence of the specific microenvironment within cervical tissue on the formation of CSCC organoids. We further compared the size and morphology of organoids cultured in Matrigel and UCEM obtained from the same patients (Fig. 4L). Both CSCC organoids cultured in Matrigel and UCEM exhibited a dense spherical structure, with the majority ranging between 100 and 200 μm in diameter (Fig. 4K). Notably, the organoids maintained a consistent size and morphology in both Matrigel and UCEM, as indicated by their circularity close to 1 (Fig. 4N). A higher circularity value is advantageous for maintaining the stability of tumor organoids. Staining results for live/dead cells revealed that CSCC organoids retained high activity in both Matrigel and UCEM after approximately 1 week of culture, with most cells demonstrating robust survival. This suggests that CSCC cells can successfully adapt to the biological microenvironment of UCEM and sustain their activity (Fig. 4, L and M). In addition, we conducted dynamic observations and comparisons of the growth process of organoids in both UCEM and Matrigel. The results demonstrated that, similar to Matrigel, CSCC organoids cultured in UCEM maintained a spherical structure and smooth morphology. Furthermore, the size of organoids in UCEM and Matrigel remained comparable throughout the growth process, with no statistically significant difference observed ($P > 0.05$; fig. S8A). Following the passage, organoids cultured in UCEM and Matrigel exhibited similar properties. Notably, cryopreserved CSCC organoids in UCEM could be successfully revived, regrown, and amplified (fig. S8B). These revived organoids retained a regular spherical structure and stable morphology, which is highly advantageous for long-term organoid culture and the establishment of a CSCC biobank. To investigate whether CSCC organoids cultured in UCEM and Matrigel maintained the structural and phenotypic characteristics of CSCC tissues, we performed H&E staining and immunohistochemical staining of multiple markers (Fig. 5) (*37*). Histological analysis showed that in both UCEM and Matrigel, the arrangement of cells in CSCC organoids was disordered, with loss of polarity, increased nuclear volume, deep staining, atypia, and disordered ratio of nuclei to cytoplasm. The basal cell–restricted marker TP63 and the cell proliferation marker KI67 were positive, indicating active cell division. The marker for persistent HPV infection, P16INK4α, was also positive, while the expression level of the cell differentiation marker KRT13 was low. These findings are consistent with the histological and immunophenotypic characteristics of CSCC and similar to those observed in native CSCC tissues. In conclusion, our experimental results suggest that UCEM can support the formation and growth of CSCC organoids and that the microenvironment specific to cervical tissue can influence the formation of these organoids. Furthermore, CSCC organoids can adapt to the ECM microenvironment provided by UCEM. UCEM enables a long-term culture of CSCC organoids without the need for Matrigel while preserving the structural and phenotypic characteristics of CSCC.

Closer transcriptional resemblance of CSCC organoids in UCEM to native tissue

To further investigate the transcriptomic characteristics of CSCC organoids cultured in UCEM, mRNA sequencing was performed on native CSCC tissues, as well as CSCC organoids cultured in Matrigel and UCEM from three patients (data S2). In three biological replicates, the mRNA coexpression in CSCC tissues, organoids cultured in Matrigel and UCEM exceeded 1×10^4 in each group (Fig. 6A). This indicates that both organoid culture methods, Matrigel and UCEM, effectively preserve the transcriptomic characteristics of native CSCC tissues. We acquired transcriptomic data of normal cervical squamous epithelial tissue from healthy women through the Genotype-Tissue Expression (GTEx) database (GTEX-S32W-1526-SM-4AD6Z, GTEX-TSE9-2726-SM-4DXSQ, GTEX-S4UY-1426-SM-4AD6Y, GTEX-TSE9-2826-SM-4DXTF) and performed principal components analysis on normal cervical squamous epithelial tissue, CSCC tissue, and organoids in Matrigel and UCEM. As shown in Fig. 6B, CSCC tissues and organoids were distinct from normal cervical squamous epithelium tissue, indicating significant differences between cervical cancer tissues and normal tissues. In tumor tissues, CSCC organoids cultured in Matrigel diverged from native CSCC tissues, while CSCC organoids cultured in UCEM showed closer similarity to native CSCC tissues, with some overlap. The heatmap of differentially expressed genes also revealed differences between CSCC organoids cultured in Matrigel and UCEM (fig. S9A), indicating that UCEM influenced the vital activities of CSCC organoids to some extent. Building upon this, we further analyzed the differentially expressed genes (fold change >2) between CSCC organoids cultured in Matrigel and UCEM. In comparison to Matrigel, 229 genes were significantly up-regulated and 70 genes were down-regulated in CSCC organoids cultured in UCEM (fig. S9B). GO enrichment analysis of the differential genes (Fig. 6D) exhibited significant enrichment of BPs (GOBP) related to immune response, signal transduction, and cell adhesion. GO cellular component (GOCC) was notably concentrated in the extracellular region, which reflects the remodeling of the ECM by tumor cells and explains how tumor evolution can provide unique niches for cancer cells to engage in altered ECM remodeling. GO molecular function (GOMF) was primarily associated with chemokines,

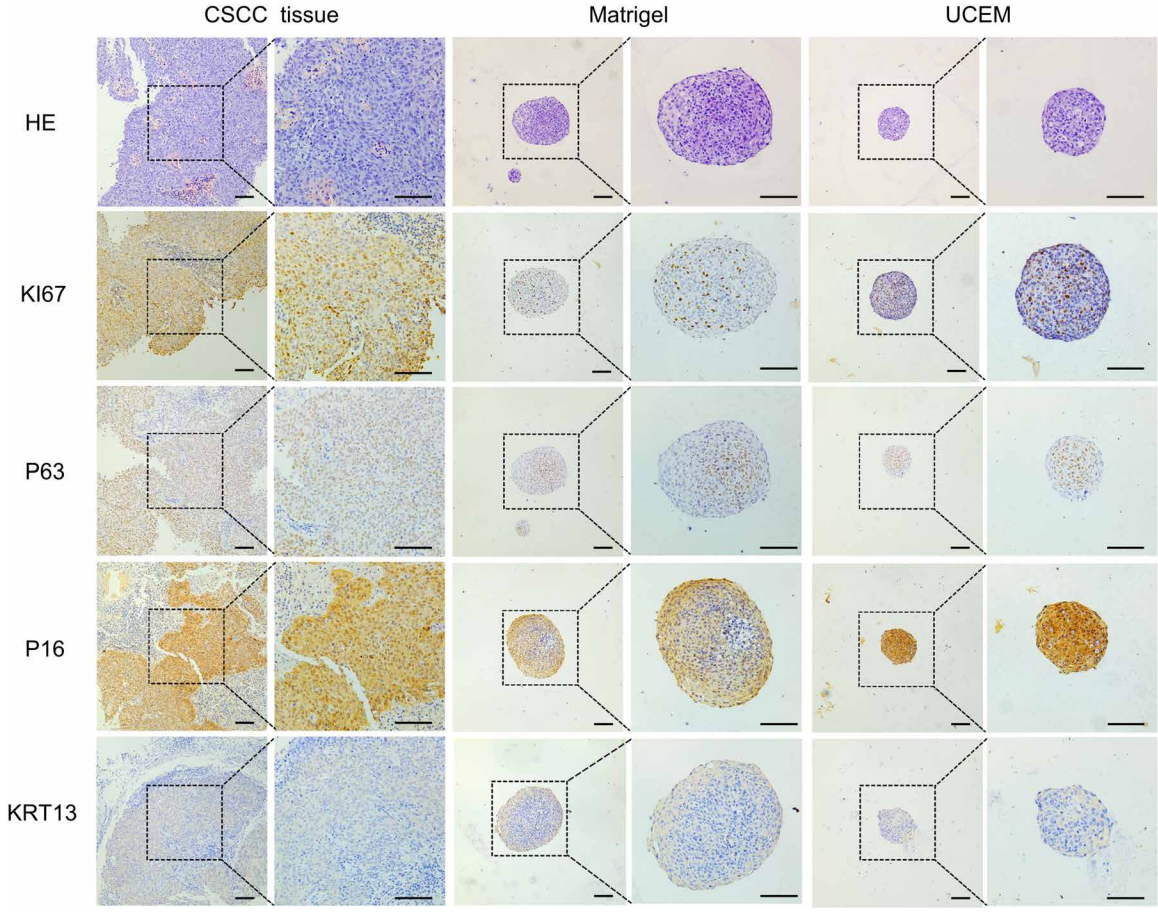

Fig. 5. Structural and phenotypic characteristics of native tumor tissue and CSCC organoids. H&E staining and immunohistochemical staining of CSCC organoids in UCEM and Matrigel showed that KI67, P63, and P16 were positive and KRT13 was weakly positive. Scale bars,100 μm.

cytokine activity regulation, receptors, and carbohydrate binding. Transcription of pro-inflammatory genes indicates the recruitment of tumor-related immune cells in vivo. KEGG enrichment analysis (Fig. 6E) demonstrated significant enrichment of signaling pathways involving viral protein-cytokine interaction and chemokine signaling. This could help elucidate the role of HPV infection and E6 and E7 virus-associated proteins in the development of cervical cancer. In addition, organoids cultured in UCEM showed significant enrichment in tumor-related signaling pathways such as nuclear factor κB (NF-κB) and tumor necrosis factor (TNF) signaling pathways. TNF-α activates NF-κB activity and regulates the expression of a series of tumor-associated genes (*38*, *39*). The NF-κB signaling pathway is normally transient and tightly regulated in normal cells. However, in cervical cancer, it becomes activated and plays a crucial role in tumor initiation, progression, and metastasis (*40*, *41*). Furthermore, we observed that several of the up-regulated genes were associated with cancer-promoting effects (fig. S9B). Building upon this, we selected well-known oncogenes implicated in cervical cancer and conducted a comparative analysis. The results indicated that the expression levels of various oncogenes involved in cervical cancer development and progression were higher in organoids cultured in UCEM compared to Matrigel, and they closely resembled those observed in CSCC-derived tissues (Fig. 6C). Not only did these genes play a role in the proliferation, invasion, and metastasis of cervical cancer cells [*NEDD9* (*42*), *EGR1* (*43*), *FPR1* (*44*), *AIF1* (*45*), and *EBI3* (*46*)] but they are also involved in the activation of immune cells and tumor-related immune regulation in CSCC tissues [*RGS1* (*47*) and *TLR10* (*48*)]. Moreover, *IFI6* expression was associated with the expression of HPV16 E7 oncoprotein (*49*). The transcriptome sequencing results demonstrated that both UCEM and Matrigel-cultured CSCC organoids retained the transcriptomic characteristics of CSCC tissues similarly. However, note that UCEM-cultured organoids outperformed Matrigel-cultured organoids in preserving multiple oncogenes and signaling pathways associated with cervical cancer, making them more akin to patient-derived CSCC tissues. These findings also suggested that the tissue-specific microenvironment might stimulate the transcription of oncogenes in primary tumor tissues.

Chemotherapy resistance in UCEM-Cultured CSCC organoids

In vitro drug trials were conducted to evaluate the response of CSCC organoids cultured in UCEM and Matrigel to chemotherapy drugs. The combination of paclitaxel and carboplatin (TC) is a commonly used chemotherapy regimen for CSCC. We compared the in vitro drug sensitivity test results with the clinical treatment response of a patient with advanced CSCC (2018 FIGO, stage IIB). CSCC organoids were cultured using patient-derived tumor tissue obtained from a biopsy

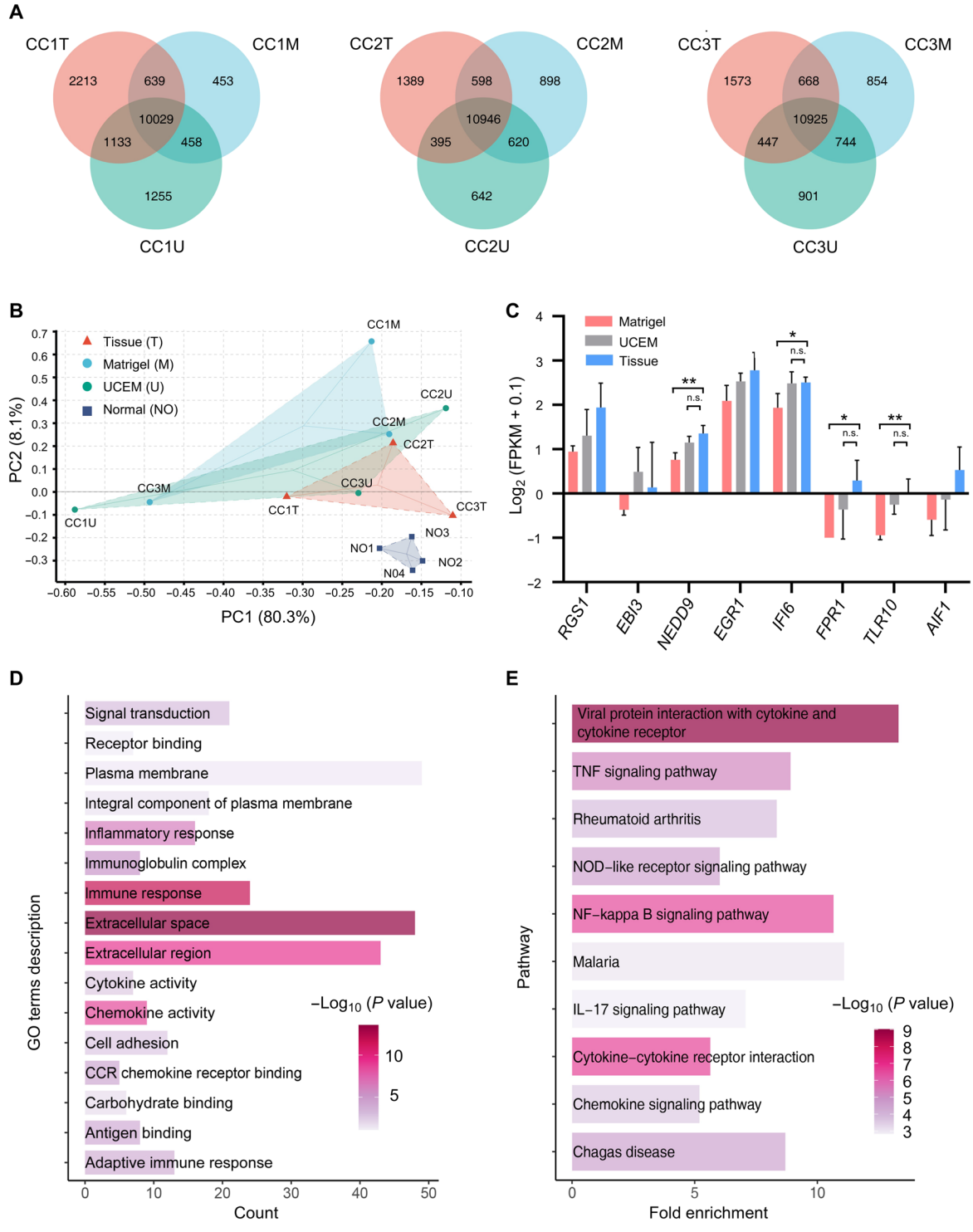

Fig. 6. Transcriptomic analysis of CSCC organoids cultured in UCEM and Matrigel. (**A**) Venn diagram of transcriptomic sequencing of three biological replicates (CC1T, CC1M, and CC1U; CC2T, CC2M, and CC2U; CC3T, CC3M, and CC3U). (**B**) Principal components analysis (PCA) of normal cervical squamous epithelium tissue from healthy female individuals (NO), primary tumor tissue (T), CSCC organoids cultured in UCEM (U), and Matrigel (M). (**C**) Comparison of highly expressed genes in CSCC between organoids and native tumor tissues, using LSD for multiple comparisons. (**D**) GO enrichment analysis of differentially expressed genes in CSCC organoids cultured in UCEM and Matrigel. (**E**) KEGG pathway enrichment analysis of differentially expressed genes in CSCC organoids cultured in UCEM and Matrigel.

and subjected to the in vitro drug sensitivity test. Following treatment with 1 μM paclitaxel combined with 10 μM carboplatin for 3 days, dissociation of CSCC organoids was observed (Fig. 7B). This finding supports the effectiveness of the TC chemotherapy regimen for this patient. Furthermore, radiographic examinations revealed a significant reduction in tumor size after treatment with the TC regimen compared to before (Fig. 7C). These results demonstrate the concordance between the treatment effect observed in our organoid model in vitro and the clinical response of the patient, which can guide the screening of chemotherapy drugs. In addition, the interaction between tumor cells and the specific microenvironment of surrounding tissues has a notable influence on tumor progression and the response to chemotherapy drugs. The use of UCEM to culture CSCC organoids allows for the establishment of a connection between the cervical tissue–specific microenvironment and cervical squamous cell cancer cells. Building upon this foundation, we compared the response to chemotherapy drugs in CSCC organoids cultured by UCEM and Matrigel under varying concentrations of carboplatin (Fig. 7A). Live/dead staining of the organoids revealed the cytotoxic effect of carboplatin at different concentrations (Fig. 7E). Following carboplatin treatment, the outer cells of the CSCC organoids perished first. As the concentration of carboplatin reached 100 μM, the growth of the organoids was significantly inhibited, resulting in a reduction in diameter. Consistently, there was a dose- and time-dependent decrease in organoid viability and proliferation in response to chemotherapy drugs (Fig. 7D). Extended exposure to chemotherapy drugs, accompanied by an increase in concentration, led to the gradual development of resistance to carboplatin in CSCC organoids cultured by UCEM, consequently resulting in higher proliferation activity compared to Matrigel. Next, we conducted a comparative analysis between in vitro drug responses of tumor organoids from 10 patients with CSCC and the clinical responses observed in matched patients. The clinical response of patients was assessed using RECIST criteria (version 1.1) through the evaluation of imaging changes before and after chemotherapy (*50*). The radiological presentation and in vitro drug sensitivity testing of patients resistant to the TC regimen were shown in fig. S10 (A and B). To test the drug response, we cultured CSCC organoids using UCEM and Matrigel and exposed them to TC regimens in vitro. The drug response curves were then plotted (fig. S10, C to F). Overall, both UCEM and Matrigel cultured CSCC organoids exhibited a strong predictive capability for patients' response to chemotherapy drugs (Fig. 7F). Notably, the IC_{50} (median inhibitory concentration) values of poor response patients (patients 6, 8, and 9) were significantly higher than those of good response patients (patients 1, 2, and 5) (Fig. 7G and data S3). Moreover, we observed that, in poor response patients, CSCC organoids cultured using UCEM displayed higher IC_{50} values compared to those cultured using Matrigel (Fig. 7G), suggesting that CSCC organoids cultured using UCEM exhibited more pronounced drug resistance and have the potential for accurate identification of drug-resistant patients. This phenomenon can be ascribed to the influence of the specific microenvironment of cervical tissue on chemotherapy drugs, alongside factors like the heightened protective effect of collagen fiber deposition on tumor cells. In addition, it is related to tumor-associated malignant biological behaviors in CSCC organoids cultured by UCEM, such as the enrichment of the NF-κB signaling pathway. Therefore, CSCC organoids cultured by UCEM hold the potential for clinical screening of antitumor drugs and serve as valuable tools for investigating the role of tissue-specific microenvironment in the development of tumor drug resistance. Moreover, this suggests that a combined therapy approach targeting tissue-specific microenvironments may offer patients the possibility of achieving deeper remission.

Preservation of CSCC tissue characteristics through xenotransplantation of organoids in UCEM

To determine whether CSCC organoids cultured in UCEM can regenerate tumor tissues in vivo, we implanted the CSCC organoids cultured in UCEM and Matrigel, obtained from the same patients, into the subcutaneous region of nude mice. Each group consisted of 10 nude mice. After 1.5 months following implantation, the nude mice were euthanized and the subcutaneous tumors were excised for comparison. The results depicted in Fig. 8A indicated that subcutaneous tumors formed in six (60.00%) nude mice in the UCEM group and seven (70.00%) nude mice in the Matrigel group, respectively. Notably, there was no statistically significant difference in the success rate of tumor formation between the two groups. Among these mice, two exclusively developed subcutaneous tumors in the Matrigel group, one solely formed subcutaneous tumors in the UCEM group, and five developed subcutaneous tumors in both groups (Fig. 8, B and C). Blood vessels were observed surrounding the subcutaneous tumor tissues in both groups (Fig. 8D and fig. S11B). We conducted a comparison of the co-occurrence of subcutaneous tumors in the two groups (Fig. 8F and fig. S11A) and performed a statistical analysis using the paired sample *t* test. The UCEM group exhibited an average volume of (54.47 ± 21.07) mm^3 with a mass of (52.32 ± 23.74) mg, while the Matrigel group displayed an average volume of (44.70 ± 31.87) mm^3 with a mass of (31.84 ± 16.91) mg. However, no statistically significant difference in the volume and mass of the subcutaneous tumors was observed between the two groups ($P > 0.05$; Fig. 8, G and H). H&E staining and immunohistochemical staining revealed that the subcutaneous tumor tissues formed by organoids in both groups resembled CSCC tissues, as indicated by the expression of the cell proliferation marker KI67 and the HPV virus infection marker P16INK4a (Fig. 8E). Furthermore, UCEM exhibited a higher presence of scattered tumor cells with positive expression of KI67 and P16INK4a, potentially attributed to the migration and proliferation of individual tumor cells in vivo. These observations served as confirmation of the proteomic characteristics of UCEM and the transcriptomic characteristics of CSCC organoids. The findings demonstrated that CSCC organoids cultured in UCEM maintained their tumorigenic properties in vivo and exhibited similarity to those cultured in Matrigel. UCEM partially replicated the migration behavior of tumor cells in the uterine cervical tissue–specific microenvironment. Notably, despite being a human-derived ECM material, UCEM did not diminish the tumorigenicity of CSCC organoids in immunodeficient mice.

DISCUSSION

The monolayer culture of CSCC tumor cells and xenotransplantation animal models is insufficient in replicating the authentic pathological state in humans, thereby limiting research on tumor pathogenesis, as well as the development of more effective therapies and drugs. The ECM is a complex structure composed of various proteins that play a crucial role in maintaining tissue function, and morphology and regulating cell phenotype, proliferation, differentiation, adhesion, motility, and signal transduction. The ECM is also a significant component of the tumor microenvironment. By providing cancer stem cell niches and regulating tumor cell growth, the ECM controls cell signaling essential to maintain tumor tissue (*51*, *52*). Tumor

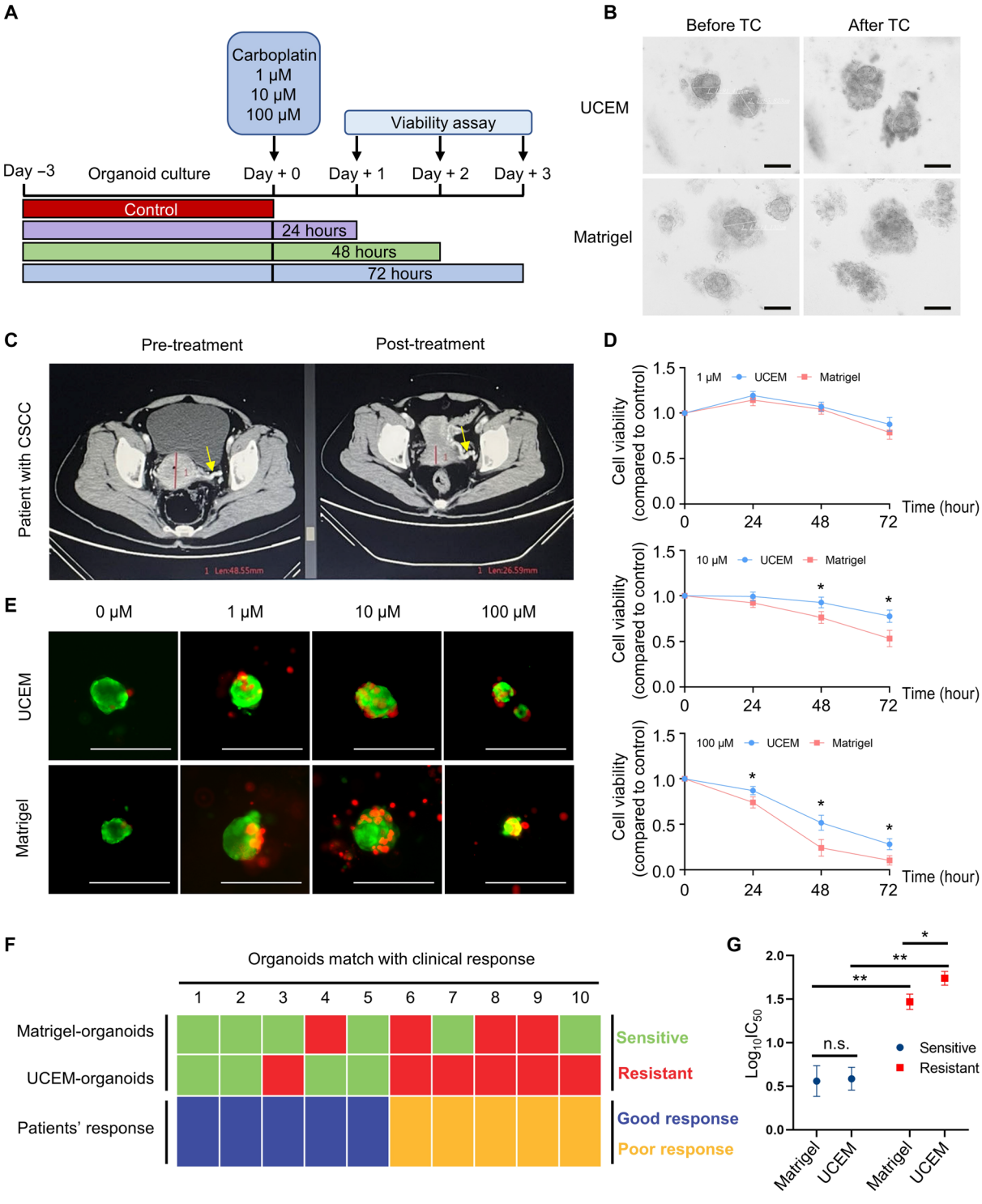

Fig. 7. Drug assay of CSCC organoids cultured by UCEM and Matrigel. (**A**) Schematic diagram of CSCC organoids treated with different concentrations of carboplatin. (**B**) The TC chemotherapy regimen induces dissociation of CSCC organoids in vitro. Scale bars, 100 μm. (**C**) The radiographic examinations (computed tomography, CT) of patients with CSCC after treatment with the TC regimen. The yellow arrow indicates the uterine artery. The red lines indicate changes in tumor size at the same plane (uterine artery level) before and after treatment. Pre-treatment: 48.55 mm, post-treatment: 26.59 mm. (**D**) Changes of CSCC organoid viability after carboplatin treatment with different concentrations. (**E**) Live/dead staining of CSCC organoids after treatment with different concentrations of carboplatin. Scale bars, 100 μm. (**F**) For patients' clinical response, blue represents sensitivity to TC regimen treatment, and yellow indicates resistance. For drug sensitivity testing using CSCC organoids in vitro, green indicates sensitivity to the TC regimen, and red indicates resistance. (**G**) Comparison of semi-inhibitory concentration ($Log_{10}IC_{50}$) in drug sensitivity testing of CSCC organoids cultured in UCEM and Matrigel.

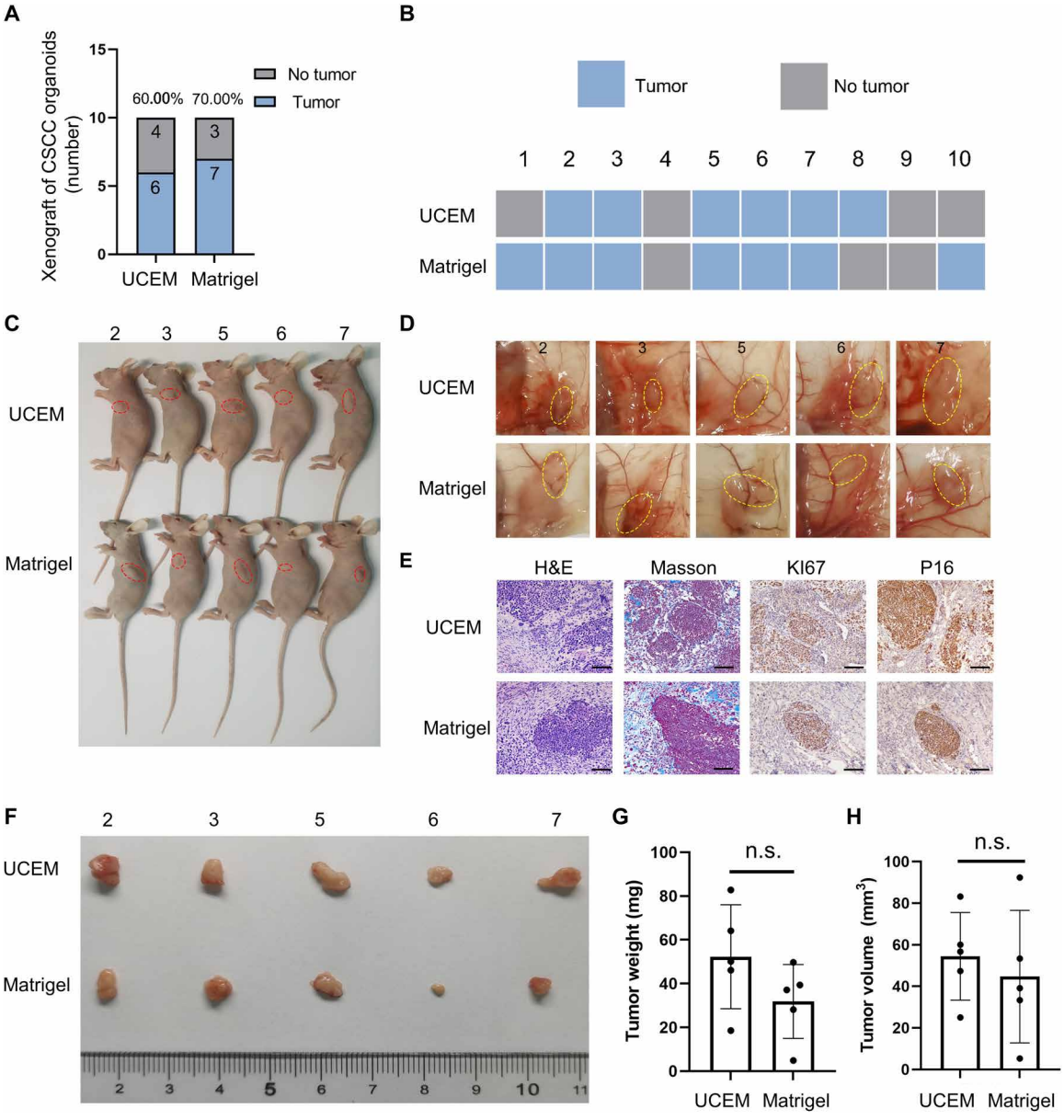

Fig. 8. Detection of tumorigenic ability of CSCC organoids in vivo. (**A**) Comparison of tumor formation rates between CSCC organoids cultured in UCEM and Matrigel in nude mice. (**B**) Tumor formation in vivo of UCEM-organoids and Matrigel-organoids derived from the same patient inoculated into two nude mice with the same number. (**C**) Simultaneous subcutaneous tumor formation of CSCC organoids cultured in UCEM and Matrigel in nude mice. (**D**) Subcutaneous tumors and surrounding blood vessels. (**E**) H&E and immunohistochemical staining of subcutaneous tumors in both groups. Scale bars, 100 μm. (**F**) Subcutaneous tumors formed by CSCC organoids cultured in UCEM and Matrigel. (**G**) Comparison of the tumor weight of subcutaneous tumors developed by organoids in UCEM and Matrigel, the difference was not statistically significant, $P > 0.05$. (**H**) Comparison of the tumor volume of subcutaneous tumors developed by organoids in UCEM and Matrigel, the difference was not statistically significant, $P > 0.05$.

progression causes ECM remodeling, leading to the interaction between reconstructed ECM and tumor cells. This interaction activates cell migration and proliferation while inhibiting cell apoptosis, thereby maintaining tumor tissue homeostasis (*53*). As a result, ECM materials not only serve as structural support for three-dimensional culture but also have significant biological activities. However, neither Matrigel, the most commonly used material, nor complex natural or synthetic chemicals can offer a tailored microenvironment for human cervical tissue, despite their applicability to organoid three-dimensional cultures. On one hand, the complex structure of the microenvironment and the wide variety of bioactive factors make it challenging to replicate artificially. On the other hand, the presence of numerous unexplored components also contributes to the difficulty. Previous studies have shown that supplementing the culture medium with decellularized hydrogel derived from porcine endometrium can enhance the proliferation of human endometrial organoids (*54*). However, this method does not eliminate the potential impact of species variations on organoids. UCEM preserves not only the uterine cervical

tissue–specific ECM microenvironment found in patients with CSCC but also eliminates potential species variations. UCEM-based CSCC organoids more accurately reflect the pathophysiological characteristics and tumor heterogeneity of patients with CSCC, having higher research value.

In cancer organoid research, we aimed to address the challenges posed by species differences and the absence of a tissue-specific microenvironment in ECM materials. To overcome these challenges, we investigated the use of decellularized ECM hydrogel derived from the para-cancerous cervix as a scaffold for the growth of CSCC organoids and compared it to the commonly used Matrigel. Our experiment involved decellularizing the cervix of patients with CSCC to obtain the ECM. We verified the removal of cell components and the retention of ECM components, such as collagen and laminin, using H&E staining and Masson staining. This decellularization method is well-established, safe, and effective and enables the preservation of the ECM in its entirety. The solidified UCEM provides the necessary anchoring and support for organoid formation.

Matrigel comprises primarily glycoproteins, constituting more than 95% of its composition, whereas collagen fibers and proteoglycans make up only 0.4 and 1%, respectively (*17*). This starkly contrasts with human tissues, where collagen serves as the primary component (*55*). The composition of UCEM includes a rich presence of type VI, I, and IV collagen fibers, aligning more closely with the structural characteristics of human tumor tissues. Collagen fibers also play a key role in the progression of cervical cancer. The elevated expression of type VI collagen fibers in cervical cancer tissues significantly correlates with tumor stage and prognosis and influences the extension, penetration, and invasion of tumor cells (*56*). Moreover, the expression level of type I collagen fibers is considerably higher in cervical cancer tissues compared to normal tissues. COL1A1, a component of type I collagen, inhibits the apoptosis of cervical cancer cells and supports tumor survival (*57*). Type IV collagen plays a critical role in tumor invasion and metastasis. As malignancy increases, collagen fibers gradually decline in the basement membrane surrounding cervical invasive carcinoma, and adjacent cancer tissues (*36*). This alteration in collagen fiber composition creates favorable conditions for tumor invasion and metastasis. Considering that organoids represent a dynamic process involving the proliferation and differentiation of tumor stem cells, UCEM effectively replicates the dynamic changes of collagen fibers during the transition of tumor tissue from low-grade malignancy to invasion, metastasis, and progressive deterioration. In summary, an ECM lacking collagen fibers is inherently incomplete. Laminin is a critical cell adhesion molecule that plays a crucial role in determining the structure and physiological function of the basement membrane (*58*). Laminin-cancer cell interactions play a critical role in tumor invasion and metastasis. Laminin promotes tumor cell proliferation and dissemination via diverse mechanisms (*28*). Our experimental results also indicated that laminin enhances the formation efficiency of CSCC organoids. These ECM structural components not only contribute to the formation of the spatial structure but also play a role in the pathogenesis and progression of cervical cancer.

EV proteins play a role in the BPs of tumorigenesis and progression. CD81, one of the markers for exosomal proteins (*59*), is found in UCEM. Our results revealed that UCEM is enriched with EV proteins that facilitate intercellular communication. Most of these proteins were significantly overexpressed in cervical cancer and associated with malignant biological behaviors. The retention of EV proteins in UCEM benefits the reflection of tumor heterogeneity and is essential for studying the pathogenesis and treatment of cervical cancers. FLNA interacts with transmembrane proteins and signaling molecules to coordinate cell adhesion and migration, while also participating in DNA damage and repair. Moreover, FLNA is significantly overexpressed in cervical cancer tissues (*60*, *61*). MYH9 was found to be highly abundant in exosomes and exhibited abnormal expression in various tumor tissues. Endogenous overexpression of MYH9 has been shown to increase tumor cell proliferation and metastasis and induce epithelial-mesenchymal transition, thereby promoting cancer progression (*62*, *63*). The expression of EEF1A1 remains highly stable in the normal cervix, cervical intraepithelial neoplasia, and invasive carcinoma and is involved in protein synthesis (*64*). Moesin (MSN) plays a crucial role in cell-cell and cell-ECM interactions, influencing cell adhesion, polarity, and migration, as well as tumor cell invasion and metastasis. In addition, high expression of MSN correlates strongly with cervical cancer malignancy and metastasis (*65*, *66*). PKM plays a pivotal role as a glycolytic enzyme that drives the conversion of glucose to lactic acid. The up-regulation of PKM expression in cervical cancer has a significant impact on the invasive, metastatic, and other malignant transformations of cervical cancer cells (*67*, *68*). Elevated levels of HSPA8 in cervical cancer significantly correlated with an unfavorable prognosis (*69*, *70*). ITGB1, a crucial integrin subunit, is essential for mediating cell-ECM interactions, thereby contributing to the formation of focal adhesions (*71*). Furthermore, various other proteins present in EVs, such as ANXA2 (*72*, *73*), TLN1 (*74*), ENO1 (*75*), and TFRC (*76*) exhibit substantial overexpression in cervical cancer. These proteins play a role in cell adhesion and movement, regulating tumor cell proliferation and metastasis, and are also linked to patient prognosis. In summary, UCEM not only preserves the structural components of the ECM but also maximizes the retention of the cervical tissue–specific ECM microenvironment, aiding in the restoration of the tumor cell niche in vivo. Preserving the retention of these bioactive proteins is advantageous for maintaining the heterogeneity of tumor tissue.

The results of isolating and culturing organoids demonstrated that UCEM effectively supports the formation and growth of CSCC organoids. The size, morphology, and proportion of living cells in organoids cultured in UCEM were comparable to those in Matrigel. Furthermore, even after subculture, cryopreservation, and resuscitation, the CSCC organoids maintained stable morphology and structure in UCEM, indicating their suitability for long-term organoid culture and biobank construction. In addition, CSCC organoids cultured in both UCEM and Matrigel retained the structure and phenotypic characteristics of CSCC tissues, as well as demonstrated similar tumorigenicity in vivo. Consequently, UCEM emerges as a viable alternative to Matrigel for CSCC organoid culture. In cancer, signals induced by the ECM influence cell phenotype and function. Notably, at the transcriptional level, the expression levels of multiple oncogenes related to cervical cancer were higher in CSCC organoids cultured with UCEM compared to Matrigel. Furthermore, the transcriptional profile of UCEM-cultured organoids more closely resembled that of native CSCC tissues, potentially due to UCEM providing both structural support and a tissue-specific microenvironment. Consequently, organoids cultured in UCEM display improved fidelity to the true pathophysiological state of CSCC in patients, thus facilitating the reflection of tumor heterogeneity. Our experimental findings indicate that the tissue-specific microenvironment can enhance the transcriptional activity of oncogenes in primary tumor tissues. Transcriptomic, histological, and clinical

data of ovarian cancer before and after chemotherapy indicate that platinum-based chemotherapy (carboplatin combined with paclitaxel) can induce tumor matrix changes in ovarian cancer patients (*77*). In solid tumors, this treatment particularly affects genes encoding core matrix proteins (collagen, proteoglycans, and ECM glycoproteins) and ECM-related proteins (*78*). In the experiment, we found that UCEM can increase the resistance of CSCC organoids to apoptosis induced by chemotherapy drugs. This indicates that the biochemical characteristics and bioactive signals of UCEM are key factors in cancer cell survival and chemotherapy resistance. Therefore, UCEM can partially optimize the pathological model of CSCC organoids, rendering them more similar to native CSCC tissues. This enhancement is particularly valuable for research into cervical cancer pathogenesis and treatment, aligning with the fundamental principles of precision medicine.

In conclusion, this experiment demonstrates that UCEM, prepared using decellularization technology, retains both the structural components of the ECM and the protein components involved in cellular activities. Therefore, UCEM effectively maintains the specific microenvironment of the ECM in human cervical tissue. Our experiment confirmed that UCEM is capable of supporting the formation and growth of CSCC organoids. Analysis of the morphology, structure, growth process, and tumorigenic ability of CSCC organoids revealed that the performance of CSCC organoids cultured in UCEM was comparable to that of Matrigel in multiple aspects. Transcriptome sequencing revealed that, when compared with Matrigel, the expression level of cervical cancer oncogenes was higher in CSCC organoids cultured in UCEM and more closely resembled that of the native CSCC tissues. Therefore, our research suggests that UCEM could enhance the tumor heterogeneity of CSCC organoids by retaining a greater number of cervical cancer oncogenes, resulting in a model that closely resembles native CSCC tissues. This offers a promising platform for studying the pathogenesis and treatment of cervical cancer and provides creative ideas for the improvement of organoid technology.

MATERIALS AND METHODS

Preparation of cervical ECM hydrogel

Para-cancerous cervical tissues from patients with CSCC were collected in multiple batches. A portion of these tissues was obtained immediately after isolating the uterine specimens. UCEM was prepared using previously reported methods (*79*). The steps involved were as follows: (i) Decellularization: The cervix was cut and digested with 0.02% pancreatin and 0.05% EDTA for 4 hours. It was then further digested in 3% Triton X-100 for 4 hours and stirred with 4% sodium deoxycholate for 4 hours to obtain white, porous cervical tissue. (ii) Disinfection and sterilization were carried out using ethanol and peracetic acid. (iii) The tissue was freeze-dried and ground into a powder. (iv) Digestion: A solution of pepsin hydrochloride was used to digest and prepare pre-gel solution (10 mg/ml). It was diluted with phosphate-buffered saline (PBS) before use and neutralized to a physiological pH of 7.35 to 7.45 using NaOH.

Characterization of cervical ECM hydrogels

Histological analysis and immunofluorescence tests were conducted on the cervix before and after the decellularization process to confirm the presence of ECM components and the absence of CCs. The cervical tissues were fixed with a 4% paraformaldehyde solution and then embedded in paraffin. Thin sections of 4 μm were cut and stained using H&E and Masson methods. H&E staining was carried out following the standard procedure, which involved hematoxylin staining for 3 min and eosin staining for 1 min. In the Masson staining procedure, the sections were soaked in a potassium dichromate solution overnight, followed by staining with Weigert's iron hematoxylin for 1 min. After rinsing with distilled water, the sections were stained with ponceau magenta for 6 min, rinsed again, immersed in a phosphomolybdic acid solution for 1 min, and stained with 2.5% aniline blue for 30 s. For immunofluorescence analysis, primary antibodies against collagen I (1:200; Abcam, ab34710), collagen IV (1:100; Abcam, ab6586), fibronectin (1:200; Abcam, ab6328), and lamininβ1 (1:100; Abcam, ab44941) were used. The primary antibodies were diluted according to the instructions and incubated overnight at 4°C. Afterward, the secondary antibody including donkey anti-rabbit (Abcam, ab150075), goat anti-rat (Abcam, ab150167), and goat anti-mouse (Abcam, ab150115) was applied and incubated at room temperature for 50 min. Subsequently, the samples were washed with PBS three times. The nucleus was stained with 4′,6-diamidino-2-phenylindole (DAPI; Servicebio, G1012) and incubated at room temperature for 10 min. Imaging was performed using the Nikon DS-U3 system equipped with fluorescence microscopy (Nikon Eclipse C1, Japan).

DNA quantification and scanning electron microscopy to observe the microstructure of UCEM

Before decellularization, the cervical tissue and ECM were freeze-dried and ground into powder. Genomic DNA was extracted and quantified using the PureLink Genomic DNA Mini Kit (Invitrogen, K182001) following the manufacturer's instructions. The DNA content in the cervical tissue and ECM was compared to confirm the successful removal of CCs. After solidification, the UCEM samples were fixed with an electron microscope fixing solution (Servicebio, G1102), rinsed three times with 0.1 M phosphate buffer (Servicebio, G0002), and then fixed with 1% osmium tetroxide (Ted Pella Inc., 18456) for 2 hours in a light-free environment. The samples underwent ethanol gradient dehydration, followed by conductive treatment after critical point drying. Last, the samples were observed and photographed under a scanning electron microscope (HITACHI, SU8100).

Oscillatory rheology

A solution (10 mg/ml) of UCEM was quiescently incubated at 37°C for 30 min. Subsequently, oscillatory rheology measurements were conducted using a rheometer (Anton Paar MCR 302e, Austria). The gap height was set to 1 mm. Amplitude (0.1 to 100 strain %) sweeps were performed on UCEM at a frequency of 1 Hz. The testing temperature was maintained at 37°C.

Protein components and functional analysis of UCEM

Mass spectrometry was used to detect and analyze the protein components in UCEM. The protein components were extracted from UCEM and then identified through liquid chromatography–mass spectrometry tandem analysis by hydrolyzing them with pancreatic enzymes. The identified proteins were subjected to systematic bioinformatics analysis using a database, which included protein annotation, functional classification, and enrichment analysis. The proteomic data of Matrigel are sourced from Suran Kim's research (*17*). Human matrisome data were obtained from (https://sites.google.com/uic.edu/matrisome/home) (*80*), while human cervical data were obtained from (www.proteinatlas.org).

Culture of cervical squamous cell carcinoma organoids in UCEM and Matrigel

This study was approved by the Ethics Committee of Zhujiang Hospital of Southern Medical University (approval number: 2023-KY-057-01). Written consent was obtained from patients before collecting samples of CSCC. Fresh tumor tissues, slightly firm in texture and pink in color, were collected from primary patients with CSCC. The tissues were obtained from biopsy or surgical specimens. The cervical cancer tissues were immediately placed in a basic culture medium (DMEM/F12, 1% penicillin/streptomycin), stored on ice, and promptly transported to the laboratory. To remove any adhering clots and mucus, the cancer tissue specimen was washed multiple times with PBS. Afterward, the cancer tissue specimen was cut into small granules using sterile scissors and digested with a solution of type IV collagenase (1 mg/ml; Gibco, catalog no. 17104019) on a shaker at 37°C for 1 hour. Digestion was terminated using a serum-free culture solution, and a cell suspension was filtered through a 100-μm filter. The cell suspension was then centrifuged to obtain cell precipitates, which were subsequently washed and centrifuged with DMEM/F12 for two to three times. Cell counting was conducted using blood cell counting plates. The cell precipitate was resuspended using growth factor–reduced Matrigel (Corning, catalog no. 356231) and UCEM (on ice). The cells were seeded into preheated 24-well plates at 25 μl per well and shaped into semispherical structures, followed by placement in a 37°C incubator for 20 to 30 min. After solidification, the CSCC organoids culture medium (BioGenous, K2169-CC) was added for group culture. The addition of Y-27632 (10 μM; Stemcell, catalog no. 72304) was used to enhance the cell survival rate. The growth of organoids was observed daily and recorded using an inverted microscope (Ningbo Shunyu, ICX41).

H&E staining and immunohistochemical staining of CSCC organoids

The CSCC tissues were fixed in 4% paraformaldehyde overnight at 4°C, followed by paraffin embedding and sectioning. The organoids were obtained by dissolving Matrigel using Cell Recovery Solution (Corning, catalog no. 354253) and then fixed with 4% paraformaldehyde overnight at 4°C. UCEM was dissolved using IV collagenase (1 mg/ml; Gibco, catalog no. 17104019), and the resulting mixture was centrifuged to obtain an organoid pellet. The pellet was then fixed with 4% paraformaldehyde overnight at 4°C. CSCC organoids were preembedded in 2% agar, paraffin-embedded, and sectioned. H&E staining, as well as immunohistochemical staining, was conducted on CSCC tissues and CSCC organoids cultured in UCEM and Matrigel. The tissues and organoids were incubated overnight at 4°C with the following antibodies: anti-P16INK4A (Abcam, catalog no. ab108349), KI67 (Abcam, catalog no. ab15580), TP63 (Abcam, catalog no. ab735), and KRT13 (Abcam, catalog no. ab92551). After incubation, a secondary antibody (ZSGB-BIO, PV-6000) was applied at room temperature for 1 hour, followed by chromogenic visualization using DAB (ZSGB-BIO, ZLI-9017). Last, the CSCC tissues and organoids were observed and photographed using a Leica DM2500 microscope.

Comparison of success rate and formation efficiency of CSCC organoids

(i) The success rate of organoid culture was compared in this study. CSCC tissue was obtained from 52 patients and CSCC organoids were cultured using Matrigel and UCEM. After 7 to 10 days, the formation of organoids was observed, and the success rate of culture was calculated using the formula: success rate of organoid culture = (number of patients successfully cultured/total number of patients) × 100%. Statistical analysis was performed using the chi-square test. (ii) The formation efficiency of organoids was compared in this study. The CSCC tissue from each patient was minced, digested, and filtered, and cell counting was conducted. Organoids were cultured using Matrigel and UCEM, respectively. The organoid formation efficiency was calculated using the formula: organoid formation efficiency (%) = (number of organoids generated/number of cells) × 100%. In a 24-well plate, each patient had three replicate wells per group, and the medium was changed every 2 to 3 days. After 7 to 10 days, the number of organoids with a diameter ≥80 μm in each well was manually counted. To minimize errors, the count was performed independently by three researchers.

Passage, cryopreservation, and resuscitation of CSCC organoids

(i) Passage: Passage of cultured CSCC organoids can be initiated after approximately 10 days. Matrigel was dissolved on ice using Cell Recovery Solution (Corning, catalog no. 354253). UCEM was dissolved with IV collagenase (Gibco, catalog no. 17104019, 1 mg/ml). The organoids were pelleted by centrifugation. The organoids were dissociated through repeated pipetting and subcultured at a ratio of 1:2 to 1:4. (ii) Cryopreservation: CSCC organoids cultured in Matrigel and UCEM were dissociated using the same method and then added to serum-free cryopreservation solution (Stemcell, catalog no. 07930) for cryopreservation. The organoids were stored at −80°C overnight and transferred to a liquid nitrogen tank for long-term storage after 24 hours. (iii) Resuscitation: CSCC organoids frozen in liquid nitrogen were removed, quickly thawed in a 37°C water bath, centrifuged with culture medium, and then embedded in Matrigel or UCEM. After solidification, they were added to the organoid culture medium.

Live/dead staining of CSCC organoids

The CSCC organoids cultured in Matrigel and UCEM were obtained following the methods described above. A live/dead cell detection solution was prepared using a centrifuge tube. First, 2 ml of PBS was added, followed by 1 μl of a 16 mM propidium iodide (PI) solution and 1 μl of a 4 mM calcein AM solution. The solution was then mixed by agitation. The resulting working solution (2 μM calcein AM and 8 μM PI) was used directly for staining. The stained organoids were incubated in a 5% CO2 cell incubator at 37°C for 30 to 40 min. Last, the organoids were observed and photographed under a fluorescence microscope.

Transcriptome sequencing analysis

mRNA transcriptome sequencing was conducted on CSCC tissues and organoids cultured in Matrigel and UCEM. The CSCC tissues and organoids originated from the same patient, and the experiment was performed with three biological replicates. The extraction and detection of RNA, library construction, quality inspection, and sequencing steps were performed by Novogene (Novogene, Beijing, China). The gene expression profiles of the organoids in Matrigel and UCEM were evaluated for their similarity to their corresponding source tissues.

Drug assay

CSCC organoids were collected and dissociated into single cells, following the passage method described above. The cells were then counted. They were resuspended in UCEM and Matrigel separately and then seeded into the wells. After solidification, an organoid culture medium was added. After 3 days of culture, the medium was

replaced with an organoid culture medium containing different concentrations of carboplatin (1, 10, and 100 μM). The viability of the organoids was assessed using CCK-8 (Dojindo, Lot. KP672) at 24, 48, and 72 hours after carboplatin treatment. The absorbance values (OD, optical density) were measured at 450 nm. Each concentration of carboplatin had three replicate wells, and a blank control was included. Patients with CSCC who underwent TC regimen chemotherapy (paclitaxel combined with carboplatin) were selected for our study. Pathological tissue samples were obtained through surgery or biopsy after obtaining informed consent from the patients. Drug sensitivity testing was performed for patients with successful organoid cultures. In combination therapy, paclitaxel (Sigma-Aldrich, catalog no. 580556) and carboplatin (Sigma-Aldrich, catalog no. 1096407) were mixed in a concentration ratio of 1:10. After 5 days of treatment with the TC protocol, the organoid activity was detected using CCK-8, and a drug response curve was plotted. In addition, the patient's clinical response was evaluated through imaging after two to four cycles of chemotherapy.

Detection of tumorigenic ability of xenotransplantation in vivo

The animal studies were conducted with the approval of the Ethics Committee of the Zhujiang Hospital of Southern Medical University (approval no. LAEC-2022-212). A total of twenty 4-week-old female nude mice of the BALB/c strain were procured and divided into two groups, with 10 mice in each group. The mice in each group were respectively inoculated with CSCC organoids which were grown in Matrigel or UCEM. A mixture solution was prepared by combining DMEM/F12 with UCEM or Matrigel in a 1:1 volume ratio. Approximately 1000 organoids with diameters <100 μm were suspended in 100 μl of the mixture solution. Following the group assignment, the organoids were implanted into the subcutaneous region of the abdominal side of the nude mice using a 1-ml syringe. Tumor volume (in cubic millimeters) was calculated as length × width^2 × 0.5, with length representing the longest tumor diameter (in millimeters) and width indicating the longest transverse diameter perpendicular to the length (in millimeters). The growth of the tumors in the nude mice was monitored for 1.5 months, and the mice were euthanized before the tumor volume reached 1500 mm^3. Subsequently, the tumor tissues were excised and photographed for comparative analysis.

Statistical analysis

The data were presented as means ± SD. The statistical analysis of the experimental data was performed using SPSS 21.0. GraphPad Prism 9.0 was used for statistical plotting, while ImageJ software was used for image analysis and quantitative assessment. The paired-samples *t* test was applied for paired data, while the two-sided Student's *t* test was used for comparing two groups when the data followed a normal distribution. The chi-square test was used for counting data, and one-way analysis of variance (ANOVA) was performed for group comparisons. A significance level of $P < 0.05$ was considered statistically significant; $^*P < 0.05$, $^{**}P < 0.01$, and $^{***}P < 0.001$.

Supplementary Materials

This PDF file includes:

Figs. S1 to S11
Table S1
Legends for data S1 to S3

Other Supplementary Material for this manuscript includes the following:

Data S1 to S3

REFERENCES AND NOTES

1. I. S. Haldorsen, N. Lura, J. Blaakær, D. Fischerova, H. M. J. Werner, What is the role of imaging at primary diagnostic work-up in uterine cervical cancer? *Curr. Oncol. Rep.* **21**, 77 (2019).
2. V. Bouvard, N. Wentzensen, A. Mackie, J. Berkhof, J. Brotherton, P. Giorgi-Rossi, R. Kupets, R. Smith, S. Arrossi, K. Bendahhou, K. Canfell, Z. M. Chirenje, M. H. Chung, M. Del Pino, S. de Sanjosé, M. Elfström, E. L. Franco, C. Hamashima, F. F. Hamers, C. S. Herrington, R. Murillo, S. Sangrajrang, R. Sankaranarayanan, M. Saraiya, M. Schiffman, F. Zhao, M. Arbyn, W. Prendiville, B. I. I. Ruiz, I. Mosquera-Metcalfe, B. Lauby-Secretan, The IARC perspective on cervical cancer screening. *N. Engl. J. Med.* **385**, 1908–1918 (2021).
3. P. A. Cohen, A. Jhingran, A. Oaknin, L. Denny, Cervical cancer. *Lancet* **393**, 169–182 (2019).
4. J. Drost, H. Clevers, Organoids in cancer research. *Nat. Rev. Cancer* **18**, 407–418 (2018).
5. N. Vasan, J. Baselga, D. M. Hyman, A view on drug resistance in cancer. *Nature* **575**, 299–309 (2019).
6. A. Fatehullah, S. H. Tan, N. Barker, Organoids as an in vitro model of human development and disease. *Nat. Cell Biol.* **18**, 246–254 (2016).
7. M. Simian, M. J. Bissell, Organoids: A historical perspective of thinking in three dimensions. *J. Cell Biol.* **216**, 31–40 (2017).
8. E. A. Aisenbrey, W. L. Murphy, Synthetic alternatives to Matrigel. *Nat. Rev. Mater.* **5**, 539–551 (2020).
9. H. K. Kleinman, G. R. Martin, Matrigel: Basement membrane matrix with biological activity. *Semin. Cancer Biol.* **15**, 378–386 (2005).
10. H. J. Lee, S. Mun, D. M. Pham, P. Kim, Extracellular matrix-based hydrogels to tailoring tumor organoids. *ACS Biomater Sci. Eng.* **7**, 4128–4135 (2021).
11. P. Lu, K. Takai, V. M. Weaver, Z. Werb, Extracellular matrix degradation and remodeling in development and disease. *Cold Spring Harb. Perspect. Biol.* **3**, a005058 (2011).
12. K. R. Levental, H. Yu, L. Kass, J. N. Lakins, M. Egeblad, J. T. Erler, S. F. Fong, K. Csiszar, A. Giaccia, W. Weninger, M. Yamauchi, D. L. Gasser, V. M. Weaver, Matrix crosslinking forces tumor progression by enhancing integrin signaling. *Cell* **139**, 891–906 (2009).
13. M. Saheli, M. Sepantafar, B. Pournasr, Z. Farzaneh, M. Vosough, A. Piryaei, H. Baharvand, Three-dimensional liver-derived extracellular matrix hydrogel promotes liver organoids function. *J. Cell. Biochem.* **119**, 4320–4333 (2018).
14. A. N. Cho, Y. Jin, Y. An, J. Kim, Y. S. Choi, J. S. Lee, J. Kim, W. Y. Choi, D. J. Koo, W. Yu, G. E. Chang, D. Y. Kim, S. H. Jo, J. Kim, S. Y. Kim, Y. G. Kim, J. Y. Kim, N. Choi, E. Cheong, Y. J. Kim, H. S. Je, H. C. Kang, S. W. Cho, Microfluidic device with brain extracellular matrix promotes structural and functional maturation of human brain organoids. *Nat. Commun.* **12**, 4730 (2021).
15. G. G. Giobbe, C. Crowley, C. Luni, S. Campinoti, M. Khedr, K. Kretzschmar, M. M. De Santis, E. Zambaiti, F. Michielin, L. Meran, Q. Hu, G. van Son, L. Urbani, A. Manfredi, M. Giomo, S. Eaton, D. Cacchiarelli, V. S. W. Li, H. Clevers, P. Bonfanti, N. Elvassore, P. De Coppi, Extracellular matrix hydrogel derived from decellularized tissues enables endodermal organoid culture. *Nat. Commun.* **10**, 5658 (2019).
16. S. Kim, Y. S. Choi, J. S. Lee, S.-H. Jo, Y.-G. Kim, S.-W. Cho, Intestinal extracellular matrix hydrogels to generate intestinal organoids for translational applications. *J. Ind. Eng. Chem.* **107**, 155–164 (2022).
17. S. Kim, S. Min, Y. S. Choi, S. H. Jo, J. H. Jung, K. Han, J. Kim, S. An, Y. W. Ji, Y. G. Kim, S. W. Cho, Tissue extracellular matrix hydrogels as alternatives to Matrigel for culturing gastrointestinal organoids. *Nat. Commun.* **13**, 1692 (2022).
18. M. R. Junttila, F. J. de Sauvage, Influence of tumour micro-environment heterogeneity on therapeutic response. *Nature* **501**, 346–354 (2013).
19. F. Gattazzo, A. Urciuolo, P. Bonaldo, Extracellular matrix: A dynamic microenvironment for stem cell niche. *Biochim. Biophys. Acta* **1840**, 2506–2519 (2014).
20. M. C. Brown, L. A. Cary, J. S. Jamieson, J. A. Cooper, C. E. Turner, Src and FAK kinases cooperate to phosphorylate paxillin kinase linker, stimulate its focal adhesion localization, and regulate cell spreading and protrusiveness. *Mol. Biol. Cell* **16**, 4316–4328 (2005).
21. F. Y. Lee, Y. Y. Zhen, C. M. Yuen, R. Fan, Y. T. Chen, J. J. Sheu, Y. L. Chen, C. J. Wang, C. K. Sun, H. K. Yip, The mTOR-FAK mechanotransduction signaling axis for focal adhesion maturation and cell proliferation. *Am. J. Transl. Res.* **9**, 1603–1617 (2017).
22. Y. Bao, L. Wang, L. Shi, F. Yun, X. Liu, Y. Chen, C. Chen, Y. Ren, Y. Jia, Transcriptome profiling revealed multiple genes and ECM-receptor interaction pathways that may be associated with breast cancer. *Cell. Mol. Biol. Lett.* **24**, 38 (2019).
23. Q. J. Zhang, D. Z. Li, B. Y. Lin, L. Geng, Z. Yang, S. S. Zheng, SNHG16 promotes hepatocellular carcinoma development via activating ECM receptor interaction pathway. *Hepatobiliary Pancreat. Dis. Int.* **21**, 41–49 (2022).
24. S. Noorolyai, N. Shajari, E. Baghbani, S. Sadreddini, B. Baradaran, The relation between PI3K/AKT signalling pathway and cancer. *Gene* **698**, 120–128 (2019).
25. A. S. Alzahrani, PI3K/Akt/mTOR inhibitors in cancer: At the bench and bedside. *Semin. Cancer Biol.* **59**, 125–132 (2019).
26. Q. Chen, L. Li, X. Liu, Q. Feng, Y. Zhang, P. Zheng, N. Cui, Hexokinases 2 promoted cell motility and distant metastasis by elevating fibronectin through Akt1/p-Akt1 in cervical cancer cells. *Cancer Cell Int.* **21**, 600 (2021).

27. Q. Song, J. Wen, W. Li, J. Xue, Y. Zhang, H. Liu, J. Han, T. Ning, Z. Lu, HSP90 promotes radioresistance of cervical cancer cells via reducing FBXO6-mediated CD147 polyubiquitination. *Cancer Sci.* **113**, 1463–1474 (2022).
28. V. Givant-Horwitz, B. Davidson, R. Reich, Laminin-induced signaling in tumor cells. *Cancer Lett.* **223**, 1–10 (2005).
29. M. Patarroyo, K. Tryggvason, I. Virtanen, Laminin isoforms in tumor invasion, angiogenesis and metastasis. *Semin. Cancer Biol.* **12**, 197–207 (2002).
30. P. Rousselle, J. Y. Scoazec, Laminin 332 in cancer: When the extracellular matrix turns signals from cell anchorage to cell movement. *Semin. Cancer Biol.* **62**, 149–165 (2020).
31. Y. Kikkawa, K. Hozumi, F. Katagiri, M. Nomizu, H. K. Kleinman, J. E. Koblinski, Laminin-111-derived peptides and cancer. *Cell Adh. Migr.* **7**, 150–159 (2013).
32. Y. Qin, C. Shembrey, J. Smith, S. Paquet-Fifield, C. Behrenbruch, L. M. Beyit, B. N. J. Thomson, A. G. Heriot, Y. Cao, F. Hollande, Laminin 521 enhances self-renewal via STAT3 activation and promotes tumor progression in colorectal cancer. *Cancer Lett.* **476**, 161–169 (2020).
33. T. D. Culp, L. R. Budgeon, M. P. Marinkovich, G. Meneguzzi, N. D. Christensen, Keratinocyte-secreted laminin 5 can function as a transient receptor for human papillomaviruses by binding virions and transferring them to adjacent cells. *J. Virol.* **80**, 8940–8950 (2006).
34. B. Skyldberg, S. Salo, E. Eriksson, U. Aspenblad, B. Moberger, K. Tryggvason, G. Auer, Laminin-5 as a marker of invasiveness in cervical lesions. *J. Natl. Cancer Inst.* **91**, 1882–1887 (1999).
35. Y. Yamada, K. Hozumi, F. Katagiri, Y. Kikkawa, M. Nomizu, Laminin-111-derived peptide-hyaluronate hydrogels as a synthetic basement membrane. *Biomaterials* **34**, 6539–6547 (2013).
36. A. Fullár, J. Dudás, L. Oláh, P. Hollósi, Z. Papp, G. Sobel, K. Karászi, S. Paku, K. Baghy, I. Kovalszky, Remodeling of extracellular matrix by normal and tumor-associated fibroblasts promotes cervical cancer progression. *BMC Cancer* **15**, 256 (2015).
37. K. Lõhmussaar, R. Oka, J. Espejo Valle-Inclan, M. H. H. Smits, H. Wardak, J. Korving, H. Begthel, N. Proost, M. van de Ven, O. W. Kranenburg, T. G. N. Jonges, R. P. Zweemer, S. Veersema, R. van Boxtel, H. Clevers, Patient-derived organoids model cervical tissue dynamics and viral oncogenesis in cervical cancer. *Cell Stem Cell* **28**, 1380–1396.e6 (2021).
38. J. Zhang, H. Wu, P. Li, Y. Zhao, M. Liu, H. Tang, NF-κB-modulated miR-130a targets TNF-α in cervical cancer cells. *J. Transl. Med.* **12**, 155 (2014).
39. L. Bai, W. Sun, Z. Han, H. Tang, CircSND1 regulated by TNF-α promotes the migration and invasion of cervical cancer cells. *Cancer Manag. Res.* **13**, 259–275 (2021).
40. J. Wu, J. Ding, J. Yang, X. Guo, Y. Zheng, MicroRNA roles in the nuclear factor kappa B signaling pathway in cancer. *Front. Immunol.* **9**, 546 (2018).
41. A. Nair, M. Venkatraman, T. T. Maliekal, B. Nair, D. Karunagaran, NF-κB is constitutively activated in high-grade squamous intraepithelial lesions and squamous cell carcinomas of the human uterine cervix. *Oncogene* **22**, 50–58 (2003).
42. N. Sima, X. Cheng, F. Ye, D. Ma, X. Xie, W. Lü, The overexpression of scaffolding protein NEDD9 promotes migration and invasion in cervical cancer via tyrosine phosphorylated FAK and SRC. *PLOS ONE* **8**, e74594 (2013).
43. J. Zhao, H. Li, M. Yuan, EGR1 promotes stemness and predicts a poor outcome of uterine cervical cancer by inducing SOX9 expression. *Genes Genomics* **43**, 459–470 (2021).
44. G. Cao, Z. Zhang, FPR1 mediates the tumorigenicity of human cervical cancer cells. *Cancer Manag. Res.* **10**, 5855–5865 (2018).
45. J. Y. Song, H. S. Bae, D. H. Koo, J. K. Lee, H. H. Jung, K. W. Lee, N. W. Lee, Candidates for tumor markers of cervical cancer discovered by proteomic analysis. *J Korean Med Sci* **27**, 1479–1485 (2012).
46. Y. M. Hou, J. Dong, M. Y. Liu, S. Yu, Expression of Epstein-Barr virus-induced gene 3 in cervical cancer: Association with clinicopathological parameters and prognosis. *Oncol. Lett.* **11**, 330–334 (2016).
47. S. Zhang, H. Wang, J. Liu, T. Tao, Z. Zeng, M. Wang, RGS1 and related genes as potential targets for immunotherapy in cervical cancer: Computational biology and experimental validation. *J. Transl. Med.* **20**, 334 (2022).
48. X. Shen, C. Wang, M. Li, S. Wang, Y. Zhao, Z. Liu, G. Zhu, Identification of $CD8^+$ T cell infiltration-related genes and their prognostic values in cervical cancer. *Front. Oncol.* **12**, 1031643 (2022).
49. C. Hua, J. Zhu, B. Zhang, S. Sun, Y. Song, S. van der Veen, H. Cheng, Digital RNA sequencing of human epidermal keratinocytes carrying human papillomavirus type 16 E7. *Front. Genet.* **11**, 819 (2020).
50. E. A. Eisenhauer, P. Therasse, J. Bogaerts, L. H. Schwartz, D. Sargent, R. Ford, J. Dancey, S. Arbuck, S. Gwyther, M. Mooney, L. Rubinstein, L. Shankar, L. Dodd, R. Kaplan, D. Lacombe, J. Verweij, New response evaluation criteria in solid tumours: Revised RECIST guideline (version 1.1). *Eur. J. Cancer* **45**, 228–247 (2009).
51. A. E. Yuzhalin, T. Urbonas, M. A. Silva, R. J. Muschel, A. N. Gordon-Weeks, A core matrisome gene signature predicts cancer outcome. *Br. J. Cancer* **118**, 435–440 (2018).
52. T. V. Tellman, M. Dede, V. A. Aggarwal, D. Salmon, A. Naba, M. C. Farach-Carson, Systematic analysis of actively transcribed core matrisome genes across tissues and cell phenotypes. *Matrix Biol.* **111**, 95–107 (2022).
53. M. W. Pickup, J. K. Mouw, V. M. Weaver, The extracellular matrix modulates the hallmarks of cancer. *EMBO Rep.* **15**, 1243–1253 (2014).
54. E. Francés-Herrero, E. Juárez-Barber, H. Campo, S. López-Martínez, L. de Miguel-Gómez, A. Faus, A. Pellicer, H. Ferrero, I. Cervelló, Improved models of human endometrial organoids based on hydrogels from decellularized endometrium. *J. Pers. Med.* **11**, 504 (2021).
55. S. Xu, H. Xu, W. Wang, S. Li, H. Li, T. Li, W. Zhang, X. Yu, L. Liu, The role of collagen in cancer: From bench to bedside. *J. Transl. Med.* **17**, 309 (2019).
56. T. Hou, C. Tong, G. Kazobinka, W. Zhang, X. Huang, Y. Huang, Y. Zhang, Expression of COL6A1 predicts prognosis in cervical cancer patients. *Am. J. Transl. Res.* **8**, 2838–2844 (2016).
57. S. Liu, G. Liao, G. Li, Regulatory effects of COL1A1 on apoptosis induced by radiation in cervical cancer cells. *Cancer Cell Int.* **17**, 73 (2017).
58. K. Miyazaki, Laminin-5 (laminin-332): Unique biological activity and role in tumor growth and invasion. *Cancer Sci.* **97**, 91–98 (2006).
59. X. Zhu, L. Long, H. Xiao, X. He, Cancer-derived exosomal miR-651 as a diagnostic marker restrains cisplatin resistance and directly targets ATG3 for cervical cancer. *Dis. Markers* **2021**, 1544784 (2021).
60. J. Yue, S. Huhn, Z. Shen, Complex roles of filamin-A mediated cytoskeleton network in cancer progression. *Cell Biosci.* **3**, 7 (2013).
61. A. Wang, L. Liu, M. Yuan, S. Han, X. You, H. Zhang, F. Lei, Y. Zhang, Role and mechanism of FLNa and UCP2 in the development of cervical cancer. *Oncol. Rep.* **44**, 2656–2668 (2020).
62. B. Wang, X. Qi, J. Liu, R. Zhou, C. Lin, J. Shangguan, Z. Zhang, L. Zhao, G. Li, MYH9 promotes growth and metastasis via activation of MAPK/AKT signaling in colorectal cancer. *J. Cancer* **10**, 874–884 (2019).
63. B. Yang, H. Liu, Y. Bi, C. Cheng, G. Li, P. Kong, L. Zhang, R. Shi, Y. Zhang, R. Zhang, X. Cheng, MYH9 promotes cell metastasis via inducing angiogenesis and epithelial mesenchymal transition in esophageal squamous cell carcinoma. *Int. J. Med. Sci.* **17**, 2013–2023 (2020).
64. Y. Shen, Y. Li, F. Ye, F. Wang, W. Lu, X. Xie, Identification of suitable reference genes for measurement of gene expression in human cervical tissues. *Anal. Biochem.* **405**, 224–229 (2010).
65. M. K. Halle, A. Sundaresan, J. Zhang, C. S. Pedamallu, V. Srinivasasainagendra, J. Blair, D. Brooke, B. I. Bertelsen, K. Woie, S. Shrestha, H. Tiwari, Y. F. Wong, C. Krakstad, A. I. Ojesina, Genomic alterations associated with mutational signatures, DNA damage repair and chromatin remodeling pathways in cervical carcinoma. *NPJ Genom. Med.* **6**, 82 (2021).
66. M. He, Y. Cheng, W. Li, Q. Liu, J. Liu, J. Huang, X. Fu, Vascular endothelial growth factor C promotes cervical cancer metastasis via up-regulation and activation of RhoA/ROCK-2/moesin cascade. *BMC Cancer* **10**, 170 (2010).
67. M. Morita, T. Sato, M. Nomura, Y. Sakamoto, Y. Inoue, R. Tanaka, S. Ito, K. Kurosawa, K. Yamaguchi, Y. Sugiura, H. Takizaki, Y. Yamashita, R. Katakura, I. Sato, M. Kawai, Y. Okada, H. Watanabe, G. Kondoh, S. Matsumoto, A. Kishimoto, M. Obata, M. Matsumoto, T. Fukuhara, H. Motohashi, M. Suematsu, M. Komatsu, K. I. Nakayama, T. Watanabe, T. Soga, H. Shima, M. Maemondo, N. Tanuma, PKM1 confers metabolic advantages and promotes cell-autonomous tumor cell growth. *Cancer Cell* **33**, 355–367 (2018).
68. L. J. Wen, X. L. Hu, C. Y. Li, J. Liu, Z. Y. Li, Y. Z. Li, J. Y. Zhou, Myosin 1b promotes migration, invasion and glycolysis in cervical cancer via ERK/HIF-1α pathway. *Am. J. Transl. Res.* **13**, 12536–12548 (2021).
69. W. Guo, H. Yu, L. Zhang, X. Chen, Y. Liu, Y. Wang, Y. Zhang, Effect of hyperoside on cervical cancer cells and transcriptome analysis of differentially expressed genes. *Cancer Cell Int.* **19**, 235 (2019).
70. M. I. Lomnytska, S. Becker, K. Hellman, A. C. Hellström, S. Souchelnytskyi, M. Mints, U. Hellman, S. Andersson, G. Auer, Diagnostic protein marker patterns in squamous cervical cancer. *Proteomics Clin. Appl.* **4**, 17–31 (2010).
71. Y. Masuda, H. Takahashi, S. Hatakeyama, TRIM29 regulates the p63-mediated pathway in cervical cancer cells. *Biochim. Biophys. Acta* **1853**, 2296–2305 (2015).
72. T. Wang, Z. Wang, R. Niu, L. Wang, Crucial role of Anxa2 in cancer progression: Highlights on its novel regulatory mechanism. *Cancer Biol. Med.* **16**, 671–687 (2019).
73. Z. Wang, C. Jiang, L. Pang, W. Jia, C. Wang, X. Gao, X. Zhang, H. Dang, Y. Ren, *ANXA2* is a potential marker for the diagnosis of human cervical cancer. *Biomark. Med.* **15**, 57–67 (2021).
74. Y. Ma, J. Liu, Z. Yang, P. Chen, D. B. Wang, CircRNA_400029 promotes the aggressive behaviors of cervical cancer by regulation of miR-1285-3p/TLN1 axis. *J. Cancer* **13**, 541–553 (2022).
75. Y. Gou, F. Li, X. Huo, C. Hao, X. Yang, Y. Pei, N. Li, H. Liu, B. Zhu, ENO1 monoclonal antibody inhibits invasion, proliferation and clone formation of cervical cancer cells. *Am. J. Cancer Res.* **11**, 1946–1961 (2021).
76. X. Xu, T. Liu, J. Wu, Y. Wang, Y. Hong, H. Zhou, Transferrin receptor-involved HIF-1 signaling pathway in cervical cancer. *Cancer Gene Ther.* **26**, 356–365 (2019).
77. E. A. Pietilä, J. Gonzalez-Molina, L. Moyano-Galceran, S. Jamalzadeh, K. Zhang, L. Lehtinen, S. P. Turunen, T. A. Martins, O. Gultekin, T. Lamminen, K. Kaipio, U. Joneborg, J. Hynninen,

S. Hietanen, S. Grénman, R. Lehtonen, S. Hautaniemi, O. Carpén, J. W. Carlson, K. Lehti, Co-evolution of matrisome and adaptive adhesion dynamics drives ovarian cancer chemoresistance. *Nat. Commun.* **12**, 3904 (2021).
78. J. Gonzalez-Molina, L. Moyano-Galceran, A. Single, O. Gultekin, S. Alsalhi, K. Lehti, Chemotherapy as a regulator of extracellular matrix-cell communication: Implications in therapy resistance. *Semin. Cancer Biol.* **86**, 224–236 (2022).
79. X. Yi, F. Liu, K. Gao, F. Chen, Y. Wang, H. Li, X. Wang, Y. Huang, H. Fu, W. Zhou, J. B. Fan, S. Wang, Y. Gao, Reconstructable uterus-derived materials for uterus recovery toward efficient live births. *Adv. Mater.* **34**, e2106510 (2022).
80. A. Naba, K. R. Clauser, S. Hoersch, H. Liu, S. A. Carr, R. O. Hynes, The matrisome: In silico definition and in vivo characterization by proteomics of normal and tumor extracellular matrices. *Mol. Cell. Proteomics* **11**, M111.014647 (2012).

Acknowledgments
Funding: This work was supported by the financial support of the National Natural Science Foundation of China (82371725 and 32301204); the Young Talent Support Project of Guangzhou Association For Science and Technology (QT-2023-021); the Science Technology Innovation Project of Foshan (FS0AAKJ218–1301-0037); Greater Bay Area Institute of Precision Medicine (Guangzhou), Fudan University, China (2023HXKT13); Key Research and Development Program of Guangzhou Municipal Science and Technology Bureau (2024B03J0379); and Guangzhou Basic and Applied Basic Research Scheme - Project for Maiden Voyage of Guangzhou Municipal Science and Technology Bureau (2024A04J4791).
Author contributions: H.S., Y.Ha., Y.C., Y.L., Yan Huang, and X.Lia. contributed to conducting experiments. H.J. and W.H. contributed to the analysis of bioinformatics. H.L., Yi Huang, X. Lv, Y.Z., and J.Z. contributed to the collection of clinical cases and samples. X.Y., X. Lin, Y.W., and H.H. contributed to designing research and writing the paper. **Competing interests:** The authors declare that they have no conflict of interest. **Data and materials availability:** All data needed to evaluate the conclusions in the paper are present in the paper and/or the Supplementary Materials.

Submitted 13 October 2023
Accepted 10 April 2024
Published 15 May 2024
10.1126/sciadv.adl3511